

# Measuring matter effects in Neutron star - Black hole binaries with Advanced LIGO: a Bayesian study

Prayush Kumar,<sup>1</sup> Michael Pürrer,<sup>2</sup> and People across the Atlantic

<sup>1</sup>*Canadian Institute for Theoretical Astrophysics, 60 St. George Street, University of Toronto, Toronto, ON M5S 3H8, Canada*<sup>\*</sup>

<sup>2</sup>*Albert Einstein Institute, Am Mühlenberg, Gölm, Germany*

(Dated: April 14, 2016)

Very recently, the Advanced LIGO (aLIGO) observatories announced the first terrestrial detection of gravitational waves. This heralds an era of observational gravitational wave (GW) astronomy. Neutron star - black hole (NSBH) binaries are one of the primary sources targeted for observation with the aLIGO detectors. GWs from these sources will carry signatures of the tidal distortion of the NS by the BH during the inspiral, and of its tidal disruption (if that happens) at merger. In the NS is disrupted, the merger and ringdown signal is drastically suppressed, which distinguishes it from a BHBH merger. In this paper, we present the first Bayesian study of the measurability of the tidal deformability of neutron stars, allowing the companion hole to take on a variety of masses and spins. First, we find that if BHBH templates are used to estimate source parameters for an NSBH signal, a significant bias is introduced in the inference if the signal-to-noise ratio (SNR) is greater than  $\rho \simeq 30$ . Second, we find that if we are to get a loud signal with  $\rho \geq 23$ , we can put a factor of two bound on the NS tidal deformability parameter  $\Lambda_{\text{NS}} \propto (R/M)^5$ . Finally, we study the improvement in our measurement of  $\Lambda_{\text{NS}}$  from multiple observations. Using an approximately astrophysical population, we find that (i) the median measured  $\Lambda_{\text{NS}}$  catches up to within 10% of the true value in approximately 20 observations; (ii) the 90% confidence interval for  $\Lambda_{\text{NS}}$  shrinks to  $\pm 50\%$  around the true value with the same number of observations. We find these results encouraging, and recommend that an effort to measure  $\Lambda_{\text{NS}}$  be taken within the LIGO-Virgo Collaboration once we begin to detect NSBH coalescences.

## I. INTRODUCTION

The Advanced LIGO (aLIGO) observatories began their first observing run “O1” mid-September 2015, operating at a factor of 3 – 4 higher gravitational-wave (GW) strain sensitivity than their first-generation counterparts [1]. During O1, the first terrestrial detection of gravitational waves was made, as was announced earlier in 2016 [2]. Emitted more than a billion year ago, these waves herald the era of observational gravitational wave (GW) astronomy as they pass through Earth. Over the 3-months of O1, aLIGO had access to more binary mergers than initial-LIGO over its entire coincident operation period. Both of aLIGO instruments will be further upgraded in phases to reach their design sensitivity by 2018 – 19, at which point we may expect to observe  $\sim 70$  binary mergers a year [3].

Coalescing binaries of compact objects, i.e. black holes (BH) and/or neutron stars (NS), remain the most interesting targets for GW based observation with aLIGO. NSBH binaries form an important sub-class of compact binaries, and we expect to observe  $\mathcal{O}(10)$  of these every year with design sensitivity aLIGO [3]. NSBH mergers are of interest for various reasons. For instance, they have been associated with (as the progenitors of) short Gamma-ray Bursts (GRBs) [4–12]. Under favorable conditions, close to merger the neutron star can get disrupted by the tidal field of its companion hole. Once disrupted, the neutron star material may form an accretion

disk around the black hole. Most of the disk matter spirals in within a few milliseconds, with a small fraction becoming unbounded and getting ejected, with a possible simultaneous burst of gamma-ray emission) [10, 11, 13–16]. A coincident detection of GWs from an NSBH system with a GRB would therefore provide us insights into the central engine powering GRBs. Another question that NSBH mergers can help answer is ‘what is the nature of matter at nuclear densities’, i.e. what is the equation of state (EoS) of neutron stars. This is what we will focus on in this paper. The gravitational-waves emitted by NSBH binaries carry subtle hints of the matter structure of the neutron star. During early inspiral, the (weak) tidal field of the companion hole deforms the star, thereby exciting its resonant oscillation modes. The induced quadrupolar moment of the star depends on the tidal field  $\mathcal{E}_{ij}$  due to its companion through the relation  $Q_{ij} = -\lambda \mathcal{E}_{ij}$ , where  $\lambda$  is the EoS dependent tidal deformability parameter related to the neutron star’s dimensionless Love number  $k_2$  and radius  $R_{\text{NS}}$  as  $\lambda := \frac{2}{3G} k_2 R_{\text{NS}}^5$ . This drains energy from the orbit resulting in an increase of the inspiral rate. We know the leading and next-to-leading order terms in post-Newtonian (PN) theory that capture this effect [17], entering binary phasing at 5PN order. Close to merger, as the NS gets disrupted and forms long tails that feed into the companion black hole, the quadrupole moment of the system falls monotonically. As a result, the emitted GWs are subdued significantly post-disruption (as compared to what they would be for a BBH), and the quasi-normal modes of the resulting black hole are not excited [13, 14, 18–20]. The difficulty in discerning NS matter effects in an NSBH coalescence

\* [prkumar@cita.utoronto.ca](mailto:prkumar@cita.utoronto.ca)

from its GW signal lies in distinguishing it reliably from a BBH signal, since the difference between the two is either subtle (during inspiral) or short-lived (disruption and merger). The earlier in inspiral the NS disrupts, the more orbits there are over which its effect is visible. The mechanism of disruption is governed by the nature of the BH, i.e. its mass and spin. More massive BHs (with  $m_{\text{BH}} \gtrsim 7 m_{\text{NS}}$ ), as well as BHs with (large) retrograde spins ( $\chi_{\text{BH}} \in [-1.0]$ ), tend to swallow the NS whole due to a rapid merger (i.e. without it disrupting before the inner-most stable circular orbit (ISCO) is reached). The quasi-normal oscillation modes of the final black hole's horizon are also excited [21]. Therefore, the only available information comes from the inspiral rate modification. On the other hand, less massive black holes spinning in the prograde sense (with mass-ratio  $q \in [2, 5]$ , and  $\chi_{\text{BH}} \geq 0$ ) can cause their companion star to disrupt much before merger, leaving a strong imprint on the emitted GW signal [14, 22–24].

A large fraction of past work aimed at measuring NS matter effects from GW signals has consisted of inquiries about binary neutron stars (BNS) [25–36]. While single observations are not as informative, Bayesian studies have shown that with 20 – 30 BNS observations, aLIGO would begin to distinguish between hard, moderate and soft candidate equations of state [37–39]. These studies rely on the PN description of BNS dynamics, which is reasonable since BNSs merge at very high frequencies and most of their signal power resides in inspiral. On the other hand, NSBHs merge at relatively lower frequencies than BNS, and their disruption during late-inspiral occurs at frequencies where aLIGO has relatively more resolving power. This, combined with a shorter inspiral, means that the merger portion of NSBH signals is relatively more valuable for measuring  $\Lambda_{\text{NS}}$ . Some past NSBH studies aimed at measuring tidal effects, however, have used PN inspiral-only waveforms [40]. In doing so, however, (i) they ignore the merger signal which could contain significant information for NSBHs, and (ii) the errors due to unknown vacuum terms in PN waveforms could easily dominate over the tidal terms themselves [41], since there are unknown point-particle terms at orders *lower* than that at which tidal effects enter. Other studies that use complete numerical simulations or derived models either use Fisher matrix to estimate  $\Lambda_{\text{NS}}$  measurement error [19, 42], which is not reliable at realistic signal-to-noise ratios (SNR) [43], or are limited in the binary parameter space they sample [21].

In this paper we study the measurability of neutron star's tidal deformability from GWs emitted by *disruptive* NSBH mergers using aLIGO. We also probe how tidal effects affect the estimation of other binary parameters for the same class of systems. This study improves upon previous work in many ways. First, we include tidal effects during inspiral and merger in a consistent way, by using the waveform model of Ref. [19] (henceforth “LEA+”). Second, we include the effect of black hole spin on tidal GW signals, in addition to the effect of BH mass and NS's

deformability itself. Third, we perform a fully Bayesian analysis, instead of using a Fisher matrix approximation. Fourth, we explore how our measurement errors decrease as we gain information from multiple (realistic) events.

We first probe the effect of not including tidal effects in parameter estimation templates on the recovery of non-tidal binary parameters, such as component masses and spins. This is the case of current and planned aLIGO efforts. To do so, we use the LEA+ model to generate a set of realistic signals, and use that as data from which we estimate binary mass and spin parameters with a Bayesian Monte-Carlo algorithm, using non-tidal (BBH) waveforms as filters. As in rest of the paper, we restrict here our parameter space to span mass-ratios  $q := m_{\text{BH}}/m_{\text{NS}} \in [2, 5]$ , black hole spin  $\chi_{\text{BH}} \in [-0.5, +0.75]$ , and dimensionless neutron star tidal deformability  $\Lambda_{\text{NS}} := G \left( \frac{c^2}{G m_{\text{NS}}} \right)^5 \lambda \in [500, 2000]$ .

The mass of NS for signals (and not templates) is fixed to  $1.35 M_{\odot}$  throughout [44], and is taken to be non-spinning [45]. Each signal is rescaled to a range of SNR values  $\rho \in [10, 70]$ . We find that non-inclusion of tidal effects leads to systematic biases in the measurement of non-tidal parameters. Consider first the binary chirp mass  $\mathcal{M}_c := M \eta^{3/5}$  where  $M$  is the binary total mass, and  $\eta := m_{\text{BH}} m_{\text{NS}} / M^2$  is the dimensionless mass-ratio. We find that for realistic (moderate) SNRs, i.e.  $\rho \lesssim 30$ , not including tidal effects introduces a barely measurable bias that remains below 50% of the statistical uncertainty of the  $\mathcal{M}_c$  measurement itself. For higher signal strengths, we find that the underlying statistical uncertainty decreases enough for the systematic bias to become comparable to it for  $\rho = 50 – 70$  and higher. This is expected because chirp mass is fairly accurately determined by the inspiral, where tidal effects are weak. Next, we consider the mass-ratio  $\eta$ . We find that only if the NS is quite deformable (with  $\Lambda_{\text{NS}} = 2000$ ), and has a companion BH whose mass is  $m_{\text{BH}} \lesssim 4.5 M_{\odot}$  (i.e. in the astrophysical “mass-gap” [46–49]), will the systematic bias in  $\eta$  measurement become comparable to its statistical uncertainties at SNRs  $\rho \leq 30$ . For SNRs  $\rho \gtrsim 30$ , however, not including tidal effects is very likely to significantly bias the mass-ratio estimate for NSBH binaries. Finally, we consider the spin on the black hole  $\chi_{\text{BH}}$ . We find that  $\chi_{\text{BH}}$  measurements are affected in a similar way to  $\eta$ . By not including tidal effects, we compromise our measurement of  $\chi_{\text{BH}}$  significantly only if signal  $\rho \gtrsim 30$ . Overall, we learn an important thing. Bayesian parameter estimation algorithms aimed at identifying NSBH binaries with low latency in order to alert electromagnetic (EM) observers in time to establish a possible coincident observation of a GRB [50–53] can use BBH templates to look for NSBH systems with aLIGO. This is so because the primary requirement of the EM follow-up effort is rapid classification of a binary as an NSBH system, which can be achieved just as easily with BBH templates, purely on the basis of the smaller component's mass. Another conclusion we draw is that detection searches are unaffected

by the choice of ignoring tidal effects in matched-filtering templates.

Next, we study the ability of aLIGO to constrain neutron star tidal deformability with a single observation of coalescing NSBHs. For this, we use the same setup and parameter choices for signal waveforms as before, but replace the template model with one that includes tidal effects from inspiral through to merger [19] (i.e. LEA+). First of all, this reduces the biases in the measurement of non-tidal parameters. Second, as we can see from Fig. 4, at signal-to-noise ratios  $\simeq 20 - 30$ , only under the most favorable circumstance (including a BH with mass within the “mass-gap”) can we put a factor of  $1.5 - 2$  bound on  $\Lambda_{\text{NS}}$  at 90% confidence level. For similar signals with  $\rho \gtrsim 30$  we can constrain  $\Lambda_{\text{NS}}$  within  $\pm 50\%$  of its true value. For more realistic SNRs and BH parameters, a single measurement is for  $\Lambda_{\text{NS}}$  is accompanied with a  $\sim \pm 150 \pm \%$ . uncertainty. While these results are expected, multiple realistic observations is the next window that we explore in order to obtain more information on  $\Lambda_{\text{NS}}$ . These results are detailed in Sec. IV.

Multiple realistic observations deliver far more information than what a single observation furnishes, as has been shown the case to be for binary neutron stars [37]. As our final study, we perform a fully-Bayesian analysis of how our estimation of  $\Lambda_{\text{NS}}$  changes as we accumulate more and more detections. The choices that determine the population are important here, and were made as follows. Neutron star mass is fixed for signals at  $1.35M_{\odot}$ , and its spin  $\chi_{\text{NS}} = 0$ . Black hole mass is sampled uniformly from the range  $[2, 5] \times 1.35 = [2.7, 6.75]M_{\odot}$ . Our choice here is given by the intersection set of the mass range that allows for neutron star disruption and the range supported by the waveform model LEA+ [16, 19, 54]. Black hole spin is sampled uniformly from the *aligned* range, i.e.  $\chi_{\text{BH}} \in [0, +1]$ . The true deformability is fixed once per population, sampled uniformly from the range  $\Lambda_{\text{NS}} \in [0, 2000]$ . In order to keep the computational cost tractable, we make a further approximation. We inject signals into zero noise at different SNRs and recover their parameters from Bayesian inferencing for a fixed set of binaries, whose parameters lie on a uniform grid given by:  $q = \{2, 3, 4, 5\} \times \chi_{\text{BH}} \equiv \{-0.5, 0, 0.5, 0.75\} \times \Lambda_{\text{NS}} \equiv \{500, 800, 1000, 1500, 2000\} \times p = \{10, 20, 30, 50, 70\}$ . Once the population parameters been selected, each event’s parameters are replaced by their nearest neighbor in the above set. We make sure that this approximation is conservative by keeping our population sampling ranges within the conservative side of the range spanned by the above set. With the caveats laid out, we report our results in Sec. V. In addition, we probe two paradigms, one that allows for BH masses to lie within the astrophysical mass-gap (paradigm A), and one that does not (paradigm B). For paradigm A, we find the following: (i) for the softer equations of state that result in less deformable neutron stars,  $15 - 20$  detections are sufficient for our median measured value of  $\Lambda_{\text{NS}}$  to lie within 10% of the true value. (ii) For NSBH populations

with more deformable NSs ( $\Lambda_{\text{NS}} \geq 1000$ ), the same is achievable within as few as 10 realistic observations. (iii) The statistical uncertainty associated with  $\Lambda_{\text{NS}}$  measurement can be restricted to be within  $\pm 50\%$  using  $10 - 20$  observations when  $\Lambda_{\text{NS}} \geq 1000$ , and using  $25 - 40$  observations for softer equations of state. All of the above is possible within a few years of design aLIGO operation [55], if astrophysical BHs do indeed have masses between  $\leq 5M_{\odot}$  (i.e. in the mass-gap). However, further restricting  $\Lambda_{\text{NS}}$  will require 50+ NSBH observations. For paradigm B, we find the information accumulation to be somewhat slower. While the quantitative inferences for  $\Lambda_{\text{NS}} \geq 1000$  populations are not affected significantly, we find  $\mathcal{O}(10 - 20)\%$  more events are required to attain the same measurement accuracy as under paradigm A. We conclude that within as few as  $20 - 30$  observations of disruptive NSBH mergers, aLIGO will begin to place interesting bounds on NS deformability. This, amongst other things, will allow us to rank different equations of state for neutron star matter from most to least likely, with a few years’ time-scale.

Finally, we note that our results are applicable for the design sensitivity LIGO instruments, that are expected to come online in 2018–19. Also note that more a recent work that improves upon the waveform model we use in this study has been published [56], but it provides only an amplitude model which needs to be (in future) augmented with a compatible phase model. In addition, accuracy of the underlying numerical simulations used to calibrate the waveform model used here have not been verified against independent codes so far. It is therefore difficult to assess the combined modeling error and its effect on our results. They are, therefore, limited by the limitations of our waveform model. However, we expect the combined effect of modeling errors to not change our qualitative conclusions.

The remainder of the paper is organized as follows. Sec. II discusses data analysis techniques and resources used in this paper, such as the waveform model, and parameter estimation algorithm. Sec. III discusses the consequences of ignoring tidal effects in parameter estimation waveform models. Sec. IV discusses the measurability for the leading order tidal parameter  $\Lambda_{\text{NS}}$  at plausible SNR values. Sec. V discusses the improvement in our measurement of  $\Lambda_{\text{NS}}$  with successive (multiple) observations of NSBH mergers. Finally, in Sec. VI we summarize our results and discuss future prospects with Advanced LIGO.

## II. TECHNIQUES

In this section we summarize various technical aspects of this paper. The model used to obtain tidal waveforms is described in Sec. II A. The process of inferring source parameters from a GW signal is summarized in Sec. II B. The process of generating and combining multiple events is instead detailed in the corresponding results section,

Sec. V.

### A. Waveform Models

In Ref. [19], the authors presented a suite of 134 numerical relativity simulations of neutron stars inspiraling into spinning black holes. Amongst the varied quantities were (a) the equation of state for the NS, (b) NS mass, (c) mass-ratio and (d) black hole spins, taken as aligned with the orbit. A total of 21 two-parameter EoSs were used for these simulations, which also had  $q \in [2, 5]$ ,  $\chi_{\text{BH}} \in [-0.5, +0.75]$ , and  $m_{\text{NS}} \in [1.20, 1.45]M_{\odot}$ . Based on this suite of simulations, the authors calibrated a frequency-domain waveform model for the inspiral and merger phasing of NSBH coalescences. The GW strain predicted by this model (henceforth ‘‘LEA’’), can be written as

$$\tilde{h}_{\text{NSBH}}(f, \vec{\theta}, \Lambda_{\text{NS}}) = \tilde{h}_{\text{BBH}}(f, \vec{\theta}) A(f, \vec{\theta}, \Lambda_{\text{NS}}) e^{i\Delta\Phi(f, \vec{\theta}, \Lambda_{\text{NS}})}, \quad (1)$$

where  $\vec{\theta} := \{m_{\text{BH}}, m_{\text{NS}}, \chi_{\text{BH}}, \chi_{\text{NS}} = 0\}$  are the intrinsic binary parameters. The first term on the right hand side is an underlying BBH waveform model that is used as a base. In the original construction of LEA, this was taken to be the SEOBNRv1 model [57] of the Effective-one-body (EOB) family [58]. The second term changes the amplitude of the BBH model to match that of an NSBH merger of otherwise identical parameters, with NS-matter effects parametrized by  $\Lambda_{\text{NS}}$ . During inspiral this term is set to unity, but is a sensitive function of  $\Lambda_{\text{NS}}$  close to merger. The third term does the same as the second, but to the waveform phasing. During inspiral,  $\Delta\Phi(f, \vec{\theta}, \Lambda_{\text{NS}})$  is set to the PN tidal phasing corrections, at the leading and next-to-leading orders [17]. Close to merger, additional phenomenological terms are added and calibrated to the 134 available NR simulations.

In this paper we use LEA for our signal and template modeling, but switch the underlying BBH model to SEOBNRv2 [59], using its reduced-order frequency-domain version [60]. We expect this change to make our conclusions more robust because: (a) the SEOBNRv2 model is more accurate [61, 62], and (b) the differences between the two EOB models are caused by the inaccuracies of SEOBNRv1 during the *inspiral* phase, many orbits before merger [61]. Since LEA only augments the inspiral phasing with PN tidal terms, our change in the underlying BBH model does not change LEA’s construction, but increases the overall model accuracy during inspiral. Therefore the model used here (‘‘LEA+’’) is a more robust version of LEA.

### B. Bayesian methods

We perform Bayesian parameter estimation for tidal signals, using both tidal and non-tidal templates. The signal parameters are selected to lie on a grid given by:

$q = \{2, 3, 4, 5\} \times \chi_{\text{BH}} = \{-0.5, 0, 0.5, 0.75\} \times \Lambda_{\text{NS}} = \{500, 800, 1000, 1500, 2000\} \times \rho = \{10, 20, 30, 50, 70\}$ . Corresponding signal waveforms are generated using the model described in the previous sub-section, and each injected into a separate zero noise data segment  $d_n$ . Templates can be either tidal or non-tidal (LEA+ with  $\Lambda_{\text{NS}} = 0$ ).

Inferred from  $d_n$ , the joint probability distribution for binary parameters  $\vec{\Theta} := \vec{\theta} \cup \{\Lambda_{\text{NS}}\}$  is given by

$$p(\vec{\Theta}|d_n, K) = \frac{p(d_n|\vec{\Theta}, K) p(\vec{\Theta}|K)}{p(d_n|K)}. \quad (2)$$

Here,  $p(\vec{\Theta}|K)$  is the prior probability for binary parameters of taking particular values. In this paper, we use a uniform prior on the individual masses within pre-chosen ranges, as well as a uniform prior on the spin of the black hole. We set neutron star’s spin = 0, and its tidal deformability parameter  $\Lambda_{\text{NS}}$  is sampled uniformly from [0, 4000]. In addition, we exclude mass-ratios between [1, 2] from our prior. This is done because of model constraints for LEA+. The prior probability of obtaining a particular realization of data  $p(d_n|K)$  is absorbed into the overall normalization. Finally, the first term in the numerator  $p(d_n|\vec{\theta}, \Lambda_{\text{NS}}, K)$  is the likelihood of obtaining the given stretch of data  $d_n$  if we assume that a signal parameterized by  $\vec{\theta} \cup \{\Lambda_{\text{NS}}\}$  is buried in it, i.e.

$$\mathcal{L}(\vec{\Theta}) \equiv p(d_n|\vec{\Theta}, K) = \mathcal{N}\exp[-(d_n - h|d_n - h)], \quad (3)$$

where  $h \equiv h(\vec{\Theta})$  is a template given by our waveform model LEA+, and the detector noise weighted inner-product  $\langle a|b \rangle$  is defined as

$$\langle a|b \rangle \equiv 4 \operatorname{Re} \left[ \int_0^\infty \frac{\tilde{a}(f)\tilde{b}(f)(f)^*}{S_n(|f|)} df \right], \quad (4)$$

where  $\tilde{a}(f)$  is the Fourier transform of the finite time series  $a(t)$ , and  $S_n(|f|)$  is the one-sided amplitude spectrum of detector noise. The definition of  $\mathcal{L}$  in Eq. 3 assumes that the instrument noise is colored Gaussian. The marginalized probability distribution for any single binary parameter (say  $\alpha$ ) can be obtained by integrating Eq. 2 over all other parameters, i.e.

$$p(\alpha|d_n, K) = \int d\vec{\Theta}_\alpha p(\vec{\Theta}|d_n, K), \quad (5)$$

where  $\vec{\Theta}_\alpha$  is the set of remaining parameters, i.e.  $\vec{\Theta}_\alpha := \vec{\Theta} - \{\alpha\}$ .

We sample the probability distribution of Eq. 2 using an ensemble sampler Markov-chain Monte-Carlo algorithm based on the `emcee` package . A total of 100 independent walkers were used, each of which was allowed to collect 100,000 samples. We measure the correlation time and keep only 20,000 independent posterior points to further analyze the calculated posterior probability distributions. One simplifying assumption made to mitigate computational cost was setting the frequency sampling rate  $\Delta f = 0.4$  Hz, which we found to be sufficient to calculate likelihoods robustly [63]. **TODO: MICHAEL.**

### III. HOW IS PE AFFECTED BY NOT INCLUDING NS MATTER EFFECTS?

Past and future GW search and source characterization efforts with Advanced LIGO have used (or plan to) BH-BH waveform templates for NS-BH mergers, ignoring the effect of the tidal deformation of the neutron star due to its companion hole on the emitted GWs. In this section we present the first fully Bayesian Monte-Carlo study of the effects of this assumption on the recovery of other physical parameters of NS-BH sources. We do so by comparing the systematic biases introduced by this assumption to the overall statistical uncertainties in the measurement of binary mass and spin parameters. We find that unless the single-detector SNR of the signal exceeds 30 (for design Advanced LIGO sensitivity), the bias accrued by ignoring tidal effects in filtering templates will remain smaller than the statistical uncertainty of the same measurement.

We first take a set of NSBH binary waveforms, which include the modeling of spin and tidal effects. Binary mass-ratio is sampled uniformly over the range  $q \in [2, 5]$  taking  $q = \{2, 3, 4, 5\}$  as our test points. The mass of the NS is fixed to  $m_{\text{NS}} = 1.35M_{\odot}$ , and therefore knowing  $q$  gives  $m_{\text{BH}}$ . The spin of the NS is fixed to zero. The spin of the BH is sampled uniformly over the range  $\chi_{\text{BH}} \in [-0.75, +0.75]$ , choosing  $\chi_{\text{BH}} \equiv \{-0.5, 0, +0.5, +0.75\}$  as our test points. Finally, we vary the deformability parameter uniformly over  $\Lambda_{\text{NS}} \in [0, 2000]$ , choosing  $\Lambda_{\text{NS}} \equiv \{500, 1000, 1500, 2000\}$  plus an additional  $\Lambda_{\text{NS}} = 800$  case. Waveform are generated for all possible combinations of these parameters, and rescaled to different strengths with  $\rho = \{20, 30, 50, 70\}$ . For all of the resulting signals, we perform a fully Bayesian parameter estimation aimed at measuring binary masses and spins from the signal. Our analysis templates differ from the signal in only one sense: all tidal terms are set to zero in the former, i.e. they correspond to BHBH mergers.

In Fig. 1 we show the ratio of the systematic bias in the measured binary chirp mass  $\mathcal{M}_c$  versus its true value, to the statistical uncertainty of the measurement itself.  $\mathcal{M}_c$  is the mass combination that occurs at leading order in the perturbative expression for GW strain from compact binaries, and is therefore very precisely measurable. Even so, we find that for  $\rho = 30$  the signal is not loud enough for the systematic bias in  $\mathcal{M}_c$  to exceed a fraction of the statistical uncertainty. When we increase the SNR to  $\rho = 50$  (middle column), we find that if we have two favorable conditions present: (a) that the BH spin be  $\gtrsim 0.4$ , and (b) the NS's true deformability be large enough that its  $\Lambda_{\text{NS}} \gtrsim 1000$ , the systematic biases from ignoring tidal effects in templates reach between 50 – 100% of the statistical uncertainty. Therefore at this signal strength, including terms involving the neutron star's internal structure in waveform models becomes increasingly gainful. At even higher SNRs, say  $\rho = 70$  (right column), under the same favorable conditions as listed above, the systematic bias in  $\mathcal{M}_c$  measurement exceeds its statistical

measurement uncertainty. If the BH is even mildly spinning, say  $\chi_{\text{BH}} \gtrsim 0.2$ , with the NS mildly deformable, say  $\Lambda_{\text{NS}} \gtrsim 800$ , we still are affected in our  $\mathcal{M}_c$  measurement at the 50% level by the use of point-particle waveform templates. Finally, we note that the measured (median)  $\mathcal{M}_c$  is always higher than its true value. This is reasonable since the tidal deformation of NSs close to merger reduces the GW signal power in high frequencies, so it would look like a BH-BH signal of a higher mass (and therefore lower merger or peak GW-power frequency).

In the next figure, Fig. 2, we show the same information (i.e. the ratio of systematic bias to statistical uncertainty in parameter measurement) for the symmetric mass-ratio  $\eta$ . Note that  $\eta$  is bounded from above and below to within  $\eta \in [0, 1/4]$ . We immediately observe that the measured (median)  $\eta$  is always lowered below its true value due to the lack of  $\Lambda_{\text{NS}}$ -dependent terms in the filter template model. This bias, as for the  $\mathcal{M}_c$  bias, decreases the merger frequency for the BH-BH template, which must better match the NS-BH merger with its quietened merger and ringdown. At SNR  $\rho = 30$  the systematic bias in  $\eta$  measurement stays mostly around 10 – 50% of its statistical measurement uncertainty. For the sole case of a very deformable NS with  $\Lambda_{\text{NS}} = 2000$ , the missing tidal pieces in template models could cause errors that are comparable to that due to noise (i.e. statistical uncertainties). For a still stronger signal with  $\rho = 50$ , we find that when the following conditions are fulfilled, the measurement of  $\eta$  is *completely compromised* due to template biases: (a) BH mass  $m_{\text{BH}} \leq 5M_{\odot}$ , (b) BH spin  $\chi_{\text{BH}} \gtrsim +0.4$ , and (c)  $\Lambda_{\text{NS}} \gtrsim 1500$ . Even under more moderate restrictions on BH and NS parameters, we find that  $\rho = 50$  is loud enough to necessitate the use of tidal-modeled templates. This observation is further strengthened if we divert our attention to the third column in Fig. 2 that presents the case for even higher SNRs ( $\rho = 70$ ).

Moving on from mass to spin parameters, we now consider the measurement of spin angular momentum of the BH  $\chi_{\text{BH}}$ . The ratio of the systematic bias introduced into and the statistical uncertainty associated with  $\chi_{\text{BH}}$  measurement is shown in Fig. 3. The presentation of information in this figure is identical to that in Fig. 1 and 2. A diverging colormap is used because both extremes of the colorbar range point to large systematic biases, while its zero (or small) value lies in the middle. For the lowest considered SNR  $\rho = 30$ ,  $\chi_{\text{BH}}$  bias is negligible, being below 50% of its statistical measurement uncertainty. For the most deformable NS structure *and* with a low-mass BH, the statistical bias in  $\chi_{\text{BH}}$  does become an important error. This is furthered at higher SNR, considering  $\rho = 50$  next (middle column of Fig. 3). We find that for low-mass BHs (with masses below  $4.5M_{\odot}$ ), the systematic measurement bias for BH spin exceeds its statistical uncertainty to become the dominant source of error. Not surprisingly, the systematic bias at both spin extremes pushes towards milder spins, since the prior excludes any more extreme spins than  $[-0.75, +0.75]$  and that pushes

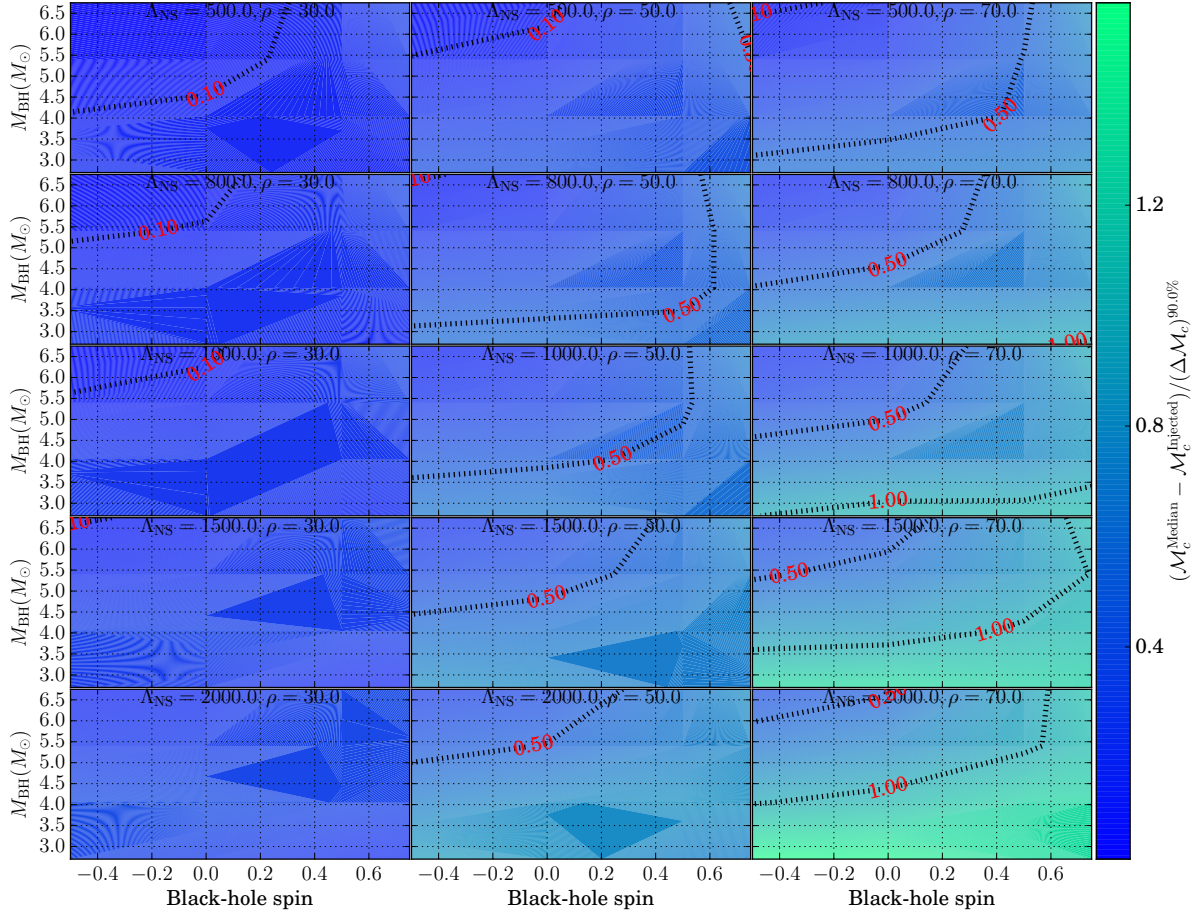


FIG. 1. We show here the ratio of systematic and statistical measurement uncertainties for the binary chirp mass over the NSBH parameter space. Each panel shows the same as a function of BH mass and spin. Across each row, we can see the effect of increasing the signal strength (i.e. SNR) with the NS's deformability fixed. Down each column, we can see the effect of the increasing NS's tidal deformability at fixed SNR. We also show dashed contours for where the ratio equals 10% (labelled “-1”) or 100% (labelled “0”). Generally, these two sources of uncertainty are different and for BBHs, the statistical errors dominate systematic ones [62]. We find that for BHNS binaries, it’s not much different until we get to high SNRs  $\rho \gtrsim 70$  for which if the BH is spinning rapidly enough, the measurement uncertainty for  $\mathcal{M}_c$  could become dominated by the exclusion of tidal effects in filtering templates.

the bulk of the posterior inwards. However as the signal’s  $\Lambda_{\text{NS}}$  is increased from  $500 \rightarrow 2000$ , low-mass BH-NS binaries with large spins on the BH show very large systematic biases in spin values, that become larger than the statistical uncertainty for  $\rho \geq 30$  and reach up to  $4\times$  the same quantity as  $\rho \rightarrow 70$ .

Summarizing these results, we find that irrespective of system parameters, below a signal-to-noise ratio of 30, our measurements of mass and spin parameters of astrophysical BHNS binaries will remain limited by the intrinsic uncertainty due to instrument noise, and do not depend on whether we include tidal effects in template models. However, when the signal-to-noise ratio exceeds 30 the systematic bias in binary mass and spin measurements become comparable to and exceed the uncertainty due to noise. Of the different parameters considered, we find that the measurement of  $\eta$  degrades worst (in

a relative-error sense) amongst all other parameters of BHNS binaries, due to the use of BH-BH waveforms in deciphering an NSBH signal.

#### IV. WHAT DO WE GAIN BY USING TEMPLATES THAT INCLUDE NS MATTER EFFECTS?

In the previous section we showed that we begin to care for the effects of NS’s deformation due to its companion hole’s tidal field, if (a) the BH is sufficiently small, (b) BH spin is aligned and  $\gtrsim +0.4$ , and (c) the NS is not very compact, with  $\Lambda_{\text{NS}} \gtrsim 1000$ . The first two conditions enhance tidal effects on emitted GWs by increasing the number of orbits at small separation, where the deviation of NSBH and BHBH dynamics is the largest.

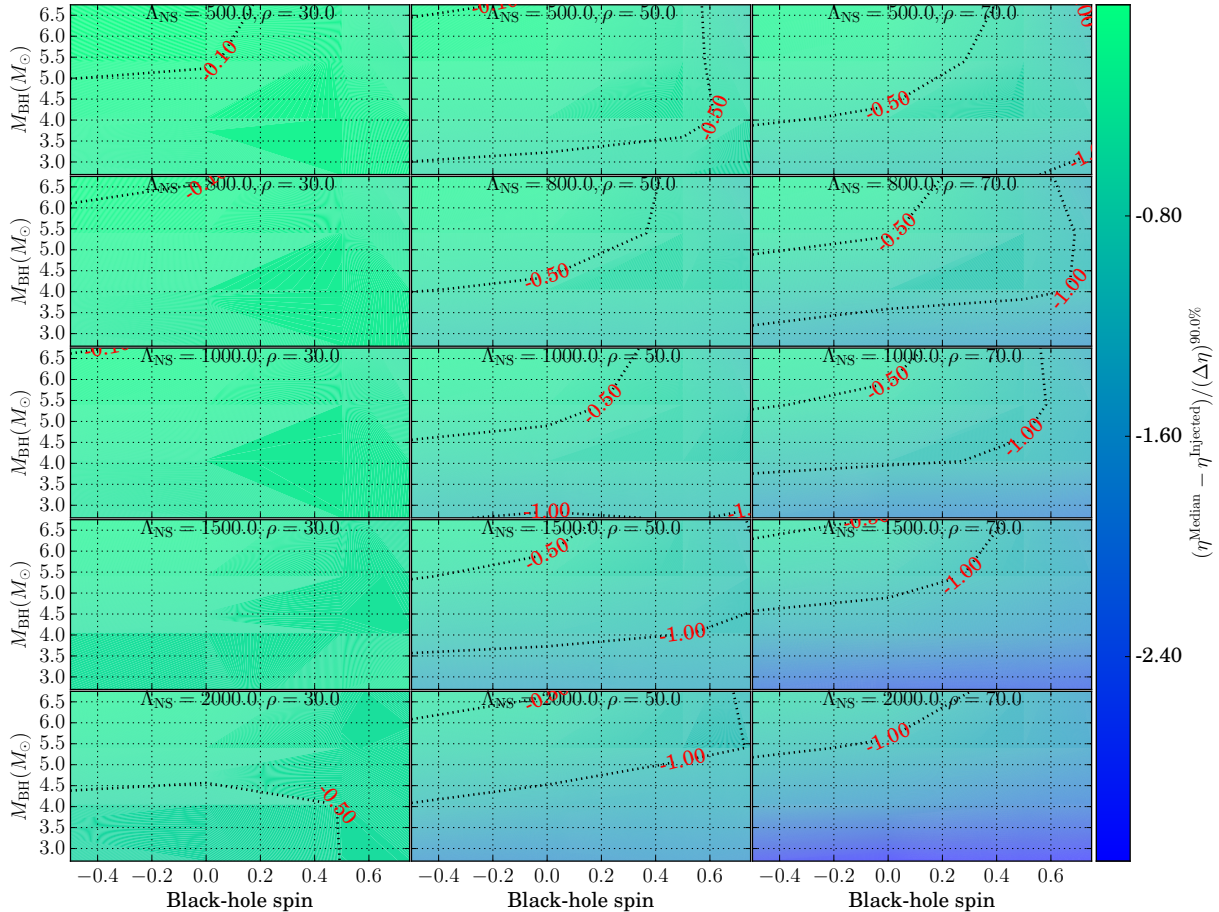


FIG. 2. This figure is similar to Fig. 1 with the difference that the quantity in question here is the symmetric mass-ratio  $\eta$ . We find that for fairly loud GW signals, with  $\rho \simeq 50$ , not including the effects of NS's tidal deformation on GW emission can become the dominant source of error for astrophysical searches with Advanced LIGO. However, for quieter signals with  $\rho \leq 30$ , it will have minimal effects on the measurement of  $\eta$ . We remind the reader that the SNRs here are all single detector values.

The third, i.e. (c), simply makes the NS more easily deformable. All of them reduce the onset frequency for NS's disruption close to merger. Therefore, systems that fulfil the above conditions have considerably (or, at least, the most) different GW morphology when compared to equivalent BHBH coalescences. Ultimately, the extent of tidal modulations of emitted GWs depends on the equation of state of neutron star matter, which becomes an indirect measurable in GW astrophysics. However, if we do indeed receive GWs from such a binary source, what information can we possibly extract from it about the internal structure of neutron stars? In this section we consider this question in perspective of measuring the tidal deformability parameter of neutron stars purely from gravitational waves they emits while orbiting spinning black holes. We find that when the BH is sufficiently spinning in the prograde sense, with  $\chi_{\text{BH}} \gtrsim +0.7$ , even at a relatively possible signal strengths ( $\rho = 20$ ), we can begin to constraint  $\Lambda_{\text{NS}}$  at the level of  $\pm 75\%$  errors with a 90% confidence level. If the signal is stronger, say  $\rho = 30$ ,

we can constraint  $\Lambda_{\text{NS}}$  better with only  $\pm 50\%$  errors, for binaries with large BH spins. This trend continues as we vary the SNR from  $\rho = 30 - 50$  upwards. In other words, with a single but moderately loud NSBH signal observation, Advanced LIGO will begin to put constraints on NS matter properties. These constraints can consequently be used to assess the likelihood of different equations of state for nuclear matter, and possibly narrow the range they span.

We use the same set of systems as in the previous section, with  $q = \{2, 3, 4, 5\}$ ,  $\chi_{\text{BH}} = \{-0.5, 0, +0.5, +0.75\}$ ,  $\Lambda_{\text{NS}} = \{500, 800, 1000, 1500, 2000\}$  and SNRs  $\rho = \{20, 30, 50, 70\}$ . For each unique combination of these parameters, we obtain a signal waveform using the tidal model of Lackey et al [19]. We use the same waveform model as input to our Bayesian parameter estimation method in order to obtain estimates for different binary parameters alongwith their full probability distributions, including for the combined NS tidal deformability param-

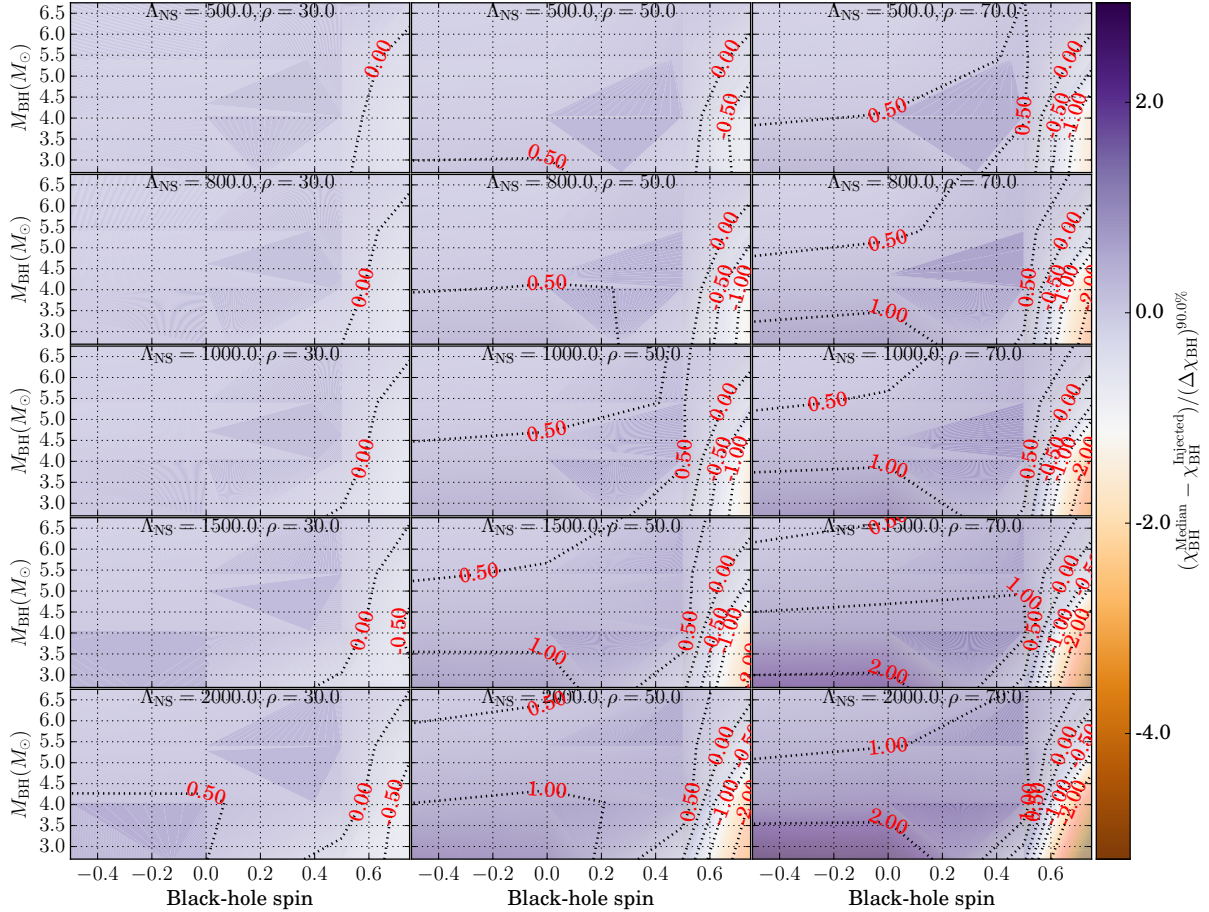


FIG. 3. This figure shows the ratio of the systematic and statistical measurement errors for BH spins, with other attributed identical to Fig. 1, and 2. Similar to the case of mass parameters, we find that below  $\rho \approx 30$ , ignoring tidal effects in templates introduces minor systematic effects, which remain subdominant to the statistical measurement uncertainties.

eter  $\Lambda_{\text{NS}}$ .

The precision with which  $\Lambda_{\text{NS}}$  can be measured is given by the width of its 90% confidence interval, as a fraction of the true value. In Fig. 4 we show the same as a function of binary parameters and signal strength. Each panel shows the percent statistical uncertainty  $\delta\Lambda$  in the measurement of  $\Lambda_{\text{NS}}$  as a function of BH masses and spins, with NS parameters and signal strength being held fixed. In each row, the signal strength is increased from left to right with  $\rho = 20 \rightarrow 70$ . In each column, the deformability of the NS is increased from top to bottom, with  $\Lambda_{\text{NS}} = 500 \rightarrow 2000$ . We find that at SNRs around  $\rho = 30$ , we begin to constrain  $\Lambda_{\text{NS}}$  meaningfully with  $\delta\Lambda \approx 100 - 150\%$ . Amongst other parameters, the BH spin and mass play a big role. A smaller BH with a larger spin always allows for a more precise measurement on  $\Lambda_{\text{NS}}$ . Visually we can see that in each panel the bottom right corner, which corresponds to low-mass BHs with large spins, is the region of smallest measurement errors on  $\Lambda_{\text{NS}}$ . The actual deformability of the NS also plays an important role on its own measurability. For e.g., when

$\Lambda_{\text{NS}} \leq 1000$ , it is fairly difficult to meaningfully constrain  $\Lambda_{\text{NS}}$  without getting remarkably lucky and finding such a binary with  $\rho \gtrsim 50$ .

In Fig. 5 we take the case of moderately deformable neutron stars, with actual  $\Lambda_{\text{NS}} = 1000$  (left panel) and 1500 (right panel), and ask how loud such a signal will have to be for us to put meaningful constraints on the tidal deformability of NSs. In the left panel, as a function BH mass and spin, we show the lowest SNR value  $\rho_c$  in order for the signal to have enough information that we can constrain  $\Lambda_{\text{NS}}$  within a factor of 2 interval (i.e. within  $\pm 100\%$ ) is a fairly modest requirement. We find promising results, which suggest that there is a fairly wide range of BH spins, less wide (but non-trivial) range of BH masses, within which if we get a moderately loud NSBH signal with  $\rho \approx 20$ , we constrain  $\Lambda_{\text{NS}}$  within a factor of 2 interval (i.e. within  $\pm 100\%$ ) around the true value. While this is not very precise, it can possibly allow us to rule out candidates for the equation of state of neutron star matter. If we want to constrain  $\Lambda_{\text{NS}}$  better

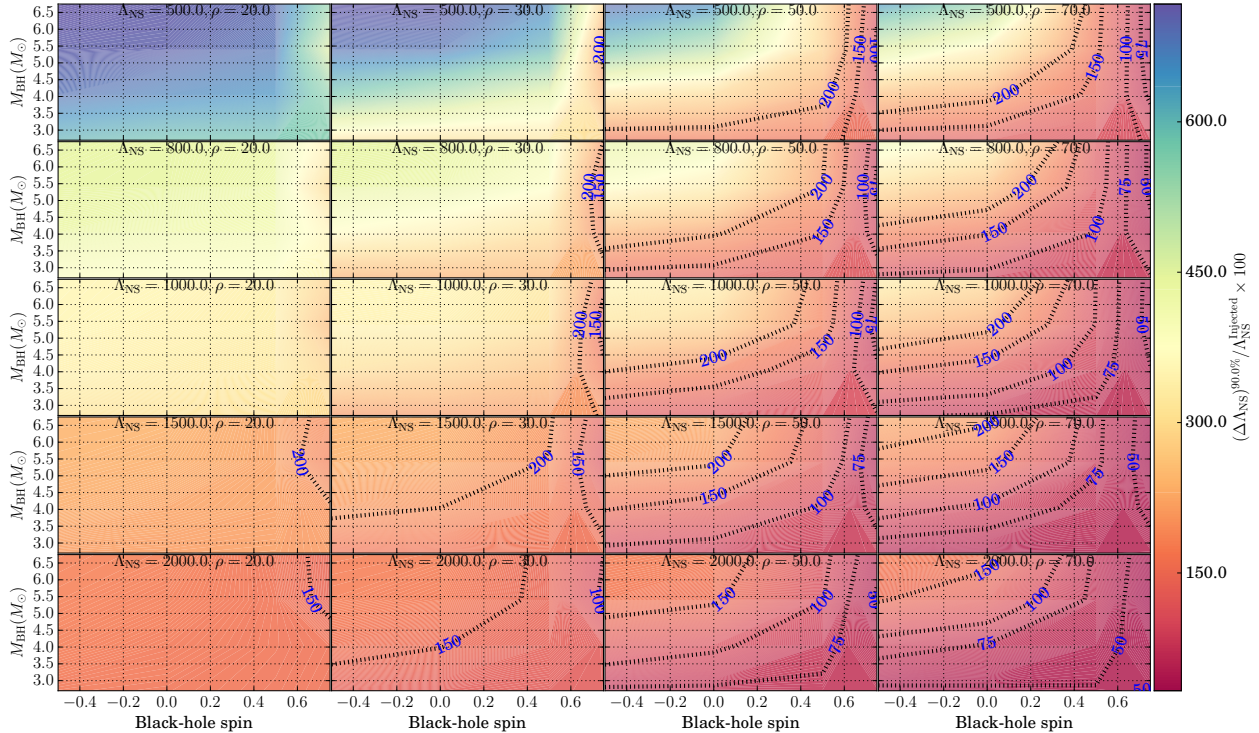


FIG. 4. This figure shows the statistical uncertainty in the measurement of  $\Lambda_{\text{NS}}$ , as a percentage of the injected signal's  $\Lambda_{\text{NS}}$  value. In each panel, the same is shown as a function of the BH mass and spin, keeping the  $\Lambda_{\text{NS}}$  and injection's SNR  $\rho$  fixed (given in the panel). Each row contains panels with the same value of  $\Lambda_{\text{NS}}$ , with  $\rho$  increasing from left to right. Each column contains panels with the same value of  $\rho$ , with  $\Lambda_{\text{NS}}$  increasing from top to bottom. Contours are drawn in each panel demarcating regions where we can constrain the  $\Lambda_{\text{NS}}$  parameter well (within a factor of two of the injected value). We note that, as expected, the measurement accuracy for  $\Lambda_{\text{NS}}$  improves with (i) increasing SNR, (ii) decreasing BH mass, (iii) increasing BH spin, and (iv) increasing  $\Lambda_{\text{NS}}$ , i.e. the tidal deformability of the neutron star.

with a single observation, however, we need SNRs of 30 or higher in each detector. This can be seen from the right panel of Fig. 5, which is similar to the left but for a higher  $\Lambda_{\text{NS}} (= 1500)$  system, with a more stringent constraint requirement that  $\Lambda_{\text{NS}}$  be measured within a factor of 1 of its true value (i.e. with  $\pm 50\%$  errors, instead of  $\pm 100\%$ ). Even for the most conducive cases, we *need* the SNR to be above 30 to reach our accuracy threshold (which is more than  $3\times$  less likely to happen than getting a signal with  $\rho = 20$ ).

Lastly, in Fig. 6 we show the conditions that BH parameters must fulfil beside having an SNR of 20 (left panel) or 30 (right panel), to obtain meaningful constraints on  $\Lambda_{\text{NS}}$ . At  $\rho = 20$ , the left panel shows that we need high BH spins  $\chi_{\text{BH}} \gtrsim +0.6$  and a very deformable NS with  $\Lambda_{\text{NS}} \geq 1500$ , in order to put a factor of 2 bound on  $\Lambda_{\text{NS}}$ . At  $\rho = 30$ , with  $\Lambda_{\text{NS}} \gtrsim 1000$  and  $\chi_{\text{BH}} \geq +0.6$  we can put a similar factor of 2 bound on  $\Lambda_{\text{NS}}$ , but with  $\chi_{\text{BH}} \sim +0.75$  and an extremely deformable NS with  $\Lambda_{\text{NS}} = 200$  one could even put a  $\pm 50\%$  errorbar on  $\Lambda_{\text{NS}}$  measurement.

In summary, with a single moderately loud BHNS observation, we could constrain the NS compactness parameter  $\Lambda_{\text{NS}}$  within  $\pm 100\%$  of its true value. To measure

better with one observation, we will need to get lucky with signals with  $\rho \geq 30$  and high BH spins, or  $\rho \geq 50$ .

## V. COMBINING OBSERVATIONS: LOOKING FORWARD WITH ADVANCED LIGO

**Multiple identical sources at low SNR:** We start with a crude calculation which tells us that approximately 8 (or 16) observations of NSBH signals with  $\rho \geq 10$  distributed uniformly in effective volume, would give us similarly accurate a measurement of  $\Lambda_{\text{NS}}$  as would a single detection with  $\rho = 50$  (or  $\rho = 70$ ).

The approximation of using (only) the dominant  $l = |m| = 2$  multipoles of gravitational-wave strain to construct the signal, ignoring other  $l \neq 2$  multipoles, has the advantage of making various angle parameters associated with the source degenerate with its distance. As a result, source distance, source sky location angles, and the inclination angle of the binary's orbital angular momentum with respect to the detector, all combine into a single “effective distance”  $D_{\text{eff}}$  that scales out as the constant amplitude factor  $1/D_{\text{eff}}$  (constant because none of the above parameters vary temporally for aligned-spin bina-

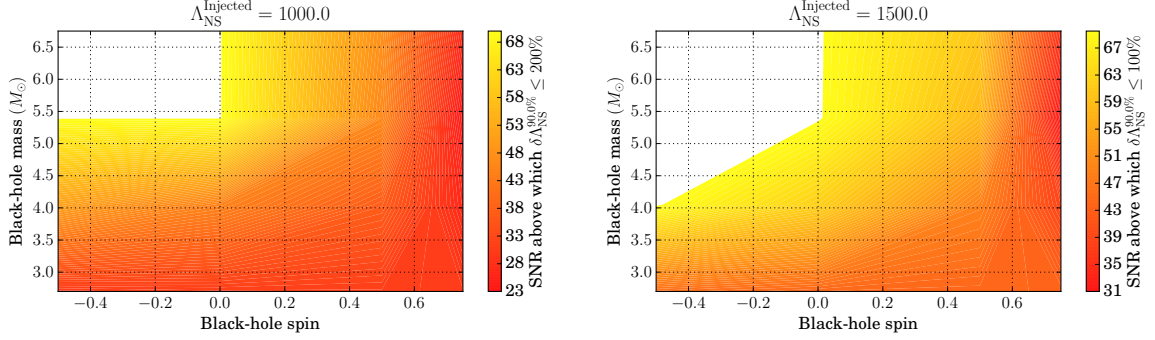


FIG. 5. In these figures we highlight the regions of BH mass and spin plane where we can constrain the  $\Lambda_{\text{NS}}$  of its companion NS within a factor of  $1 - 2$  of its true value. Panels correspond to different signal strength, with  $\rho$  increasing from left to right. Within each panel,  $\Lambda_{\text{NS}}$  measurement uncertainty contours are shown as functions of BH mass and spin, with line-types corresponding to different uncertainty levels, and colors showing the injected  $\Lambda_{\text{NS}}$ . As hinted at in Fig. 4, we note that the measurability of NS matter effects improves with all factors that enhances the signature of the NS's disruption on the *detectable* portion of the emitted GW signal (implying, within a frequency band set by the detectors).

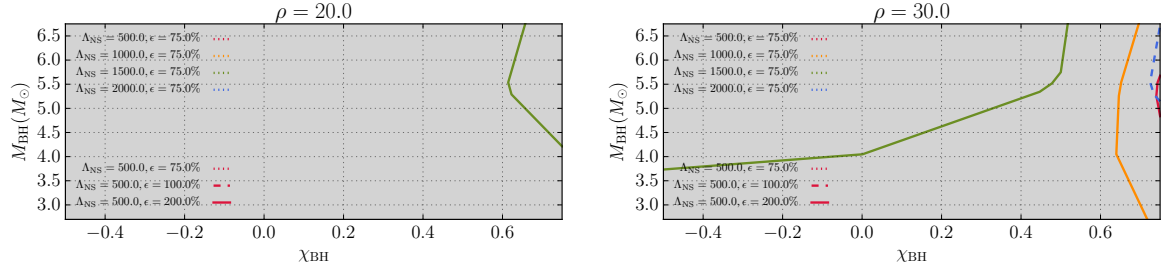


FIG. 6. In these figures we highlight the regions of BH mass and spin plane where we can constrain the  $\Lambda_{\text{NS}}$  of its companion NS within a factor of  $1 - 2$  of its true value. Panels correspond to different signal strength, with  $\rho$  increasing from left to right. Within each panel,  $\Lambda_{\text{NS}}$  measurement uncertainty contours are shown as functions of BH mass and spin, with line-types corresponding to different uncertainty levels, and colors showing the injected  $\Lambda_{\text{NS}}$ . As hinted at in Fig. 4, the measurability of NS tidal deformability improves with all factors that enhances the signature of the NS's disruption on the *detectable* portion of the emitted GW signal (implying, within a frequency band set by the detectors).

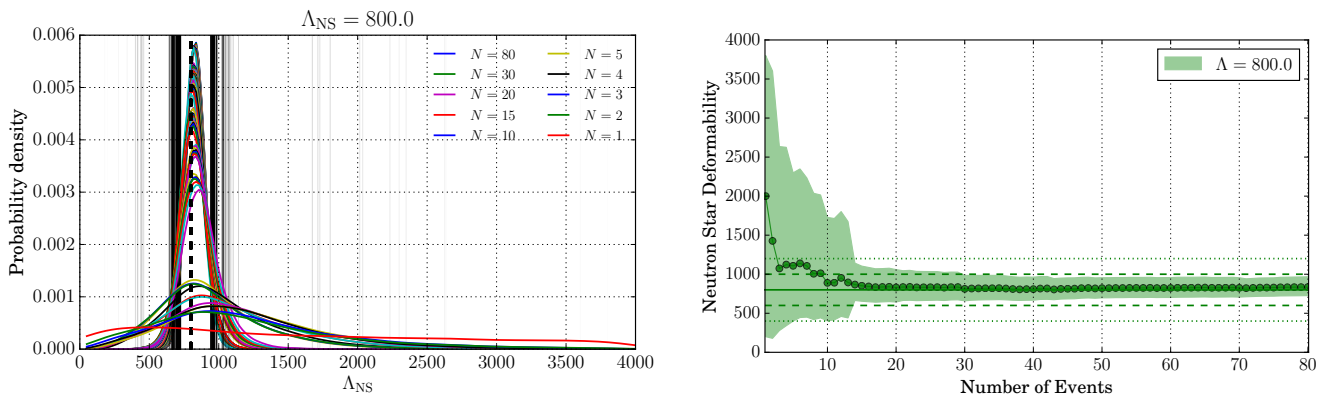


FIG. 7. These panels show the accumulation of information from a population whose  $\Lambda_{\text{NS}} = 800$ . *Left:* Posterior probability distributions for  $\Lambda_{\text{NS}}$  (colored curves), and associated 90% confidence intervals (grey vertical lines), shown for different number of accumulated observations  $N$ . Distributions are normalized to unit area. *Right:* Measured median value of  $\Lambda_{\text{NS}}$  (as solid circles) and the associated 90% confidence intervals (as the vertical extent of filled region), shown as a function of number of observations  $N$ . Solid horizontal line indicates the true value of  $\Lambda_{\text{NS}}$ . Dashed and dotted horizontal lines (a pair for each line-style) demarcate  $\pm 25\%$  and  $\pm 50\%$  error bounds.

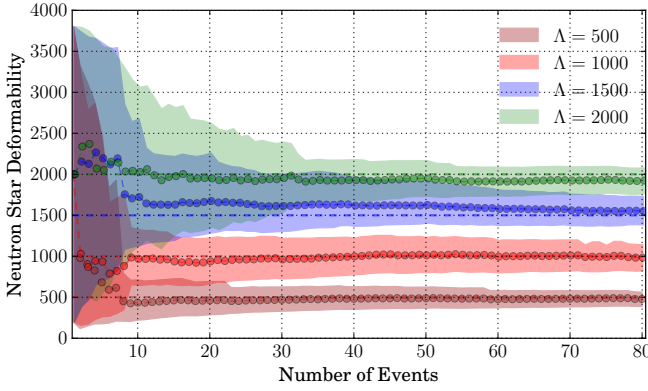


FIG. 8. In this figure, the filled regions show how our measurement of  $\Lambda_{\text{NS}}$  improves as the number of observed events ( $N$ , shown on  $x$ -axis) increases. Each color corresponds to an independent population with its true value of  $\Lambda_{\text{NS}}$  given in the legend. For each population, we show the median measured  $\Lambda_{\text{NS}}$  value (as filled circles), as well as the associated 90% confidence intervals for the measurement (as the vertical extent of the filled region about the median), as functions of  $N$ .

ries). In order to consider multiple events, let's imagine a population uniformly distributed in effective volume, i.e. within a sphere of radius  $D_{\text{eff}}^{\max}$ . The radius of this sphere is set by the lowest SNR that is distinguishable from noise by LIGO searches. Now, divide the sphere into  $I$  shells of equal thickness. The radius of the  $i$ -th shell would then be  $D_i = D_{\text{eff}}^{\max}(i - 1/2)/I$ . The measurement uncertainty in  $\Lambda_{\text{NS}}$  scales inversely with SNR, and hence directly with the effective distance to the source. Therefore, if we have a measurement error  $\sigma_0$  for a source located at  $D_{\text{eff}} = D_0$ , the same error for the same source located within the  $i$ -th shell would be  $\sigma_i = \sigma_0 \frac{D_i}{D_0}$ . The combined error from independent measurements of  $\Lambda_{\text{NS}}$  for identical sources at different distances is given by

$$\frac{1}{\sigma^2} = \sum_{i=1}^I \frac{N_i}{\sigma_i^2} = \left( \frac{D_0}{\sigma_0} \right)^2 \sum_{i=1}^I \frac{N_i}{D_i^2}, \quad (6)$$

where  $N_i$  is the number of sources detected in the  $i$ -th shell. Continuing on this line of inquiry, Ref. [30] found the root-mean-square averaged measurement error from  $\langle N \rangle := \langle \sum N_i \rangle$  sources distributed uniformly in effective volume within a sphere of radius  $D_{\text{eff}}^{\max}$  to be

$$\sigma_{\text{avg}} := \frac{1}{\sqrt{\langle 1/\sigma^2 \rangle}} = \frac{\sigma_0}{D_0} D_{\text{eff}}^{\max} \frac{1}{\sqrt{3\langle N \rangle}}, \quad (7)$$

given a fiducial pair  $(\sigma_0, D_0)$ . It is straightforward to deduce from Eq. 7 that the same measurement certainty as afforded by a single observation with a high SNR  $\rho_c$  can be obtained from  $N = \rho_c^2/300$  observations uniformly distributed in effective volume with SNRs  $\geq 10$ . E.g., to

get to the level of certainty afforded at SNR = 70, we would need  $49/3 \approx 16 - 17$  realistic detections.

There are two main caveats to this rudimentary calculation, first outlined in Ref. [30]: (i) it applies to identical sources, which is astrophysically next to impossible to achieve exactly, but could perhaps happen approximately; (ii) the combined average measurement error  $\sigma_{\text{avg}}$  has been defined as in the first equality in Eq. 7. To overcome both, we next perform a Bayesian population analysis.

**Astrophysical source population:** Imagine that we have  $N$  stretches of data,  $d_1, d_2, \dots, d_N$ , each containing a single signal emitted by an NSBH binary. Each of these signals can be characterized by the following binary parameters:  $\vec{\theta} = \{m_{\text{BH}}, m_{\text{NS}}, \chi_{\text{BH}}, \chi_{\text{NS}}, \rho\} \cup \{\Lambda_{\text{NS}}\}$ . Note that we have folded in the luminosity distance, inclination angle of the binary's orbital angular momentum with respect to the plane of the detector, and source's sky location angles into a single parameter  $\rho$ , which is the SNR of the received signal. This is possible because of our simplification of using only the dominant  $l = |m| = 2$  modes of the GW strain <sup>1</sup> that makes various angle parameters completely degenerate with distance. Further, let  $K$  denote all of our collective prior knowledge, except for expectations on binary parameters themselves, which enter the following calculation explicitly. For instance,  $K$  includes our assumption that all NS's in a single population have the same deformability parameter  $\Lambda_{\text{NS}}$ , and its cumulative measurement is therefore possible. Using Bayes' theorem, the measured probability distribution function for  $\Lambda_{\text{NS}}$  from  $N$  observations is given by <sup>2</sup>

$$p(\Lambda_{\text{NS}}|d_1, d_2, \dots, d_N; K) = p(\Lambda_{\text{NS}}|K)^{1-N} \prod_{i=1}^N p(\Lambda_{\text{NS}}|d_i, K), \quad (8)$$

where  $p(\Lambda_{\text{NS}}|K)$  is the prior expectation for  $\Lambda_{\text{NS}}$ , and all  $N$  observations are taken to be mutually independent. A priori, we assume that no particular value of  $\Lambda_{\text{NS}}$  is preferred over another, and  $\Lambda_{\text{NS}} \leq 4000$ , i.e.

$$p(\Lambda_{\text{NS}}|K) = \frac{1}{4000} \text{Rect}\left(\frac{\Lambda_{\text{NS}} - 2000}{4000}\right). \quad (9)$$

In the second set of terms in Eq. 8 (of the form  $p(\Lambda_{\text{NS}}|d_i, K)$ ), each is the probability distribution for  $\Lambda_{\text{NS}}$  inferred *a posteriori* from the  $i$ -th observation in isolation. They are calculated by integrating

$$p(\Lambda_{\text{NS}}|d_i, K) = \int d\vec{\theta} p(\vec{\theta}, \Lambda_{\text{NS}}|d_i, K), \quad (10)$$

<sup>1</sup> The  $l = |m| = 2$  multipoles of the GW strain, when decomposed in a spin  $-2$  weighted spherical harmonic basis, contain more than 99% of the total signal power

<sup>2</sup> Eq. 8 includes the following implicit factor to normalize its right-hand side:  $\frac{\prod_i p(d_i|K)}{\int p(\Lambda_{\text{NS}}) p(d_1, d_2, \dots, d_N|\Lambda_{\text{NS}}; K) d\Lambda_{\text{NS}}}$

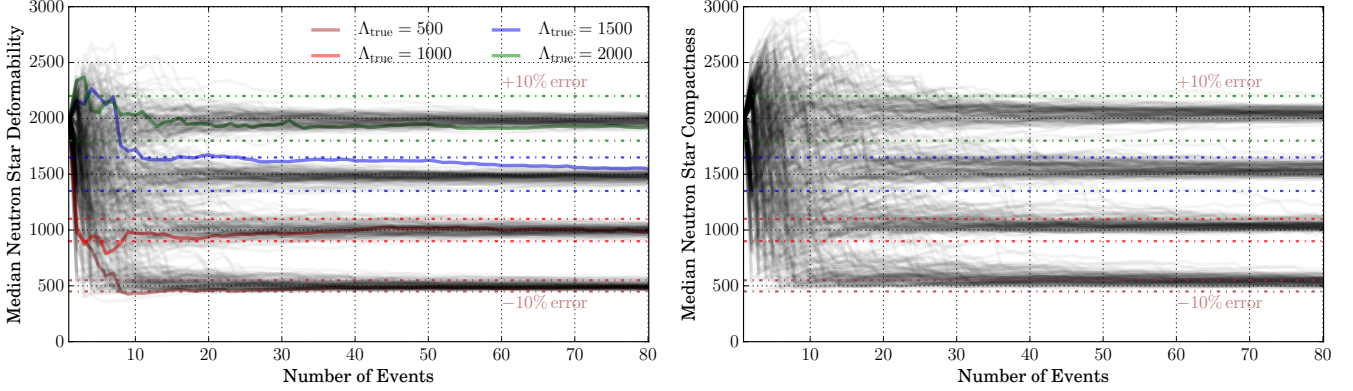


FIG. 9. *Left:* This figure shows the median value of the recovered probability distribution for  $\Lambda_{\text{NS}}$ , as a function of the number of events in the population  $N$ . There are four family of curves, one corresponding each to  $\Lambda_{\text{NS}} = \{500, 1000, 1500, 2000\}$ , with 100 independent populations within each family. One curve in each family is highlighted in color, representing that it is the same population as was illustrated in Fig. 7–8. In the same color we show  $\pm 10\%$  error-bounds on  $\Lambda_{\text{NS}}$  with horizontal dash-dotted lines. We observe that within  $10 - 25$  observations, the median of the measured cumulative probability distribution for  $\Lambda_{\text{NS}}$  will lie within  $10\%$  of the true value. *Right:* This figure is identical to the left panel, with the only difference that the BH masses in each population are restricted to lie *outside* the astrophysical mass-gap (i.e. paradigm B). The difference that we observe under this paradigm is that we need more ( $30+$ ) events to achieve the same ( $10\%$ ) measurement accuracy for populations with  $\Lambda_{\text{NS}} < 1000$ . For more deformable neutron stars,  $10 - 25$  events would suffice.

where  $p(\vec{\theta}, \Lambda_{\text{NS}} | d_n, K)$  is the inferred joint probability distribution of all source parameters  $\vec{\theta} \cup \{\Lambda_{\text{NS}}\}$  for the  $i$ -th event, as given by Eq. 2. By substituting Eq. 9–10 into Eq. 8, we calculate the probability distribution for  $\Lambda_{\text{NS}}$  as measured using  $N$  independent events.

Our goal is to understand the improvement in our measurement of  $\Lambda_{\text{NS}}$  with the number of recorded events. To do so, we simulate populations of  $N$  observations each, and quantify what we learn from each successive observation using Eq. 8. For each population, we determine how rapidly our median estimate for  $\Lambda_{\text{NS}}$  converges to the true value, and how rapidly our confidence intervals for the same shrink, with increasing  $N$ . In order to generate each population, we first fix the NS properties: (i) NS mass  $m_{\text{NS}} = 1.35M_{\odot}$ , (ii) NS spin  $\chi_{\text{NS}} = 0$  and (iii) NS tidal deformability  $\Lambda_{\text{NS}} = \text{fixed value chosen from } \{500, 800, 1000, 1500, 2000\}$ . Each event is generated independently, sampling the remaining source parameters uniformly from the following ranges: (i) mass-ratio  $q \in [2, 5]$ , (ii) BH spin  $\chi_{\text{BH}} \in [0, 0.75]$ , (iii) effective distance from within a spherical volume whose radius is given by the lowest detectable SNR (which we take as  $\rho = 10$ ). We remind ourselves that once binary parameters are fixed, there is a one-to-one mapping between effective distance and SNR. Additionally, we consider an alternate population paradigm (paradigm B, with paradigm A being the standard one described above), where populations are generated as above but further restricting mass-ratios such that source BH masses lie *outside* the astrophysical mass-gap [46–49]. Finally, in order to mitigate computational cost, we make an additional simplification. We perform full Bayesian parameter estimation for a set of simulated signals whose parameters are the vertices of

the following regular hypercubic grid (henceforth “G”):  $q = \{2, 3, 4, 5\} \times \chi_{\text{BH}} = \{-0.5, 0, 0.5, 0.75\} \times \Lambda_{\text{NS}} = \{500, 800, 1000, 1500, 2000\} \times \rho = \{10, 20, 30, 50, 70\}$ . The final population is given by substituting all of the  $N$  events, generated as above, with their respective nearest neighbours on the parameter grid G.

In Fig. 7 we show illustrative results for a single population of  $N = 80$  events. The neutron star deformability is fixed at  $\Lambda_{\text{NS}} = 800$  for all events. In the left panel, each curve shows the probability distributions for  $\Lambda_{\text{NS}}$  as inferred from  $N$  events, with  $N$  ranging from  $1 - 80$ . We also mark the  $90\%$  confidence intervals associated with each of the probability distribution curves. From the figure, we can visualize information accumulation. The first few observations do not have enough information to bound  $\Lambda_{\text{NS}}$  (with  $90\%$  confidence) much more than our prior from Eq. 9 does. However, the median of these cumulative distributions appears to track the true value of  $\Lambda_{\text{NS}}$  rapidly. In the right panel, we present information derived from the left panel. The line-circle curve shows the measured median from  $N$  observations, with the latter on the  $x$ -axis. The pair of dashed (dotted) horizontal lines mark  $\pm 25\%$  ( $\pm 50\%$ ) error bars. At each  $N$ , the range spanned by the filled region is the  $90\%$  confidence interval deduced from the same events. This figure somewhat quantifies the qualitative deductions we made from the left panel. We find that the measured median does track the true value quickly, reaching  $10\%$  accuracy with  $10 - 15$  observations. With the same information, our confidence intervals also shrink to  $\pm 25\%$ . In Fig. 8 we show further results from 4 independent populations, with the source  $\Lambda_{\text{NS}}$  alone changing between them. The sampled values, i.e.  $\Lambda_{\text{NS}} = \{500, 1000, 1500, 2000\}$ , range

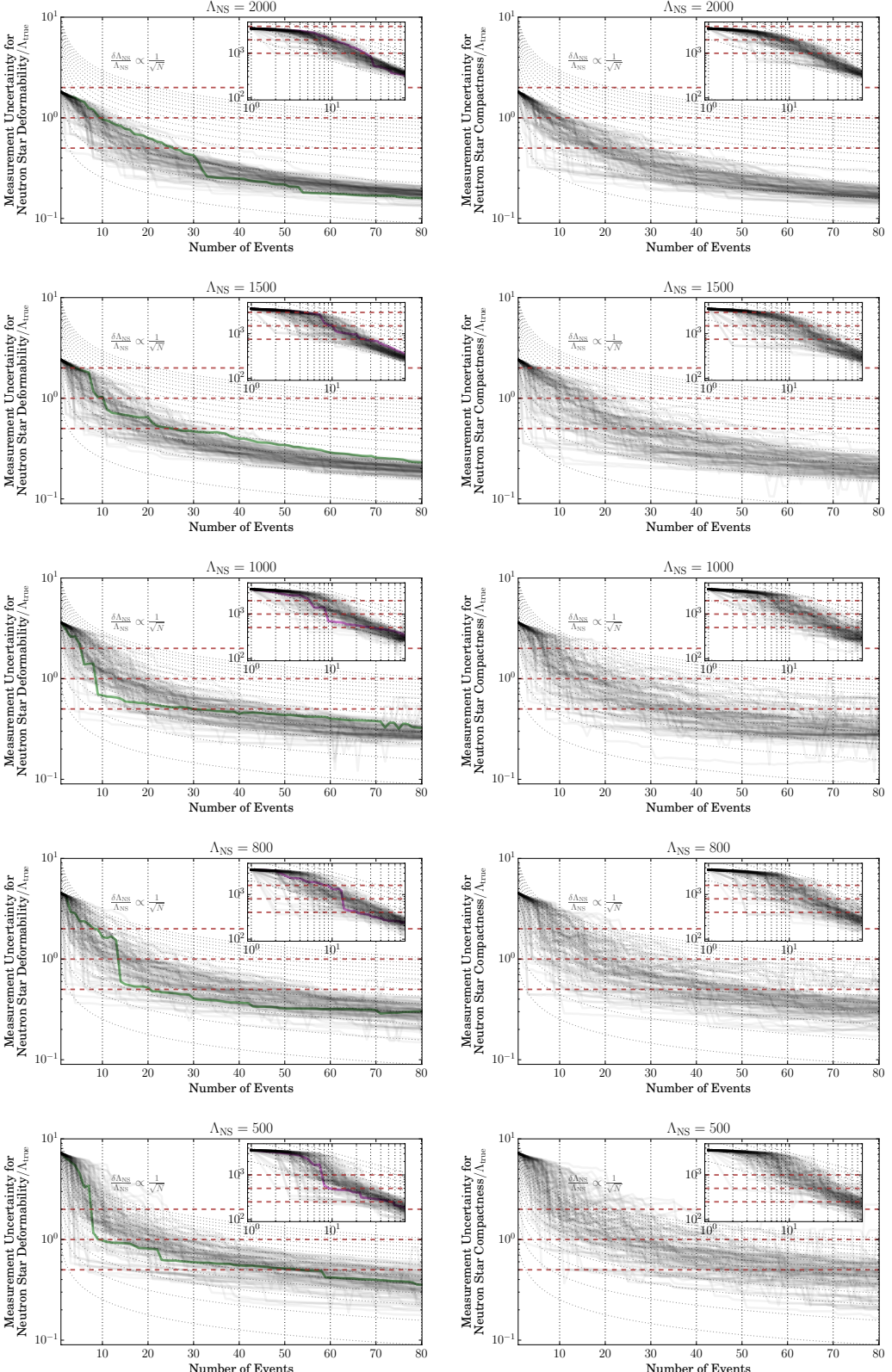


FIG. 10. These figures show the width of the 90% confidence interval for  $\Lambda_{\text{NS}}$  (normalized by its true value), as a function of the number of observed events  $N$ . The left column panels show populations sampled under paradigm A, which allows BH masses to fall within the astrophysical mass-gap, while those on the right show populations drawn under paradigm B which respects the mass-gap. Each panel corresponds to a unique value of populations'  $\Lambda_{\text{NS}}$ , decreasing from 2000  $\rightarrow$  500 as we go from top to bottom. In each panel, 100 curves are shown, each corresponding to an independent population draw. The one colored curve in each panel highlights the population used in Fig. 7-8. The insets in each panel show the same information, with the ordinate *not* normalized by the true value of  $\Lambda_{\text{NS}}$ . We find that with approximately 25 or so events, we begin to put statistically meaningful constraints on  $\Lambda_{\text{NS}}$ , restricting it to within  $\pm 50\%$  of the true value. We can expect to achieve this with a few years of design aLIGO operation [55]. Further tightening of the confidence intervals will require 40+ events.

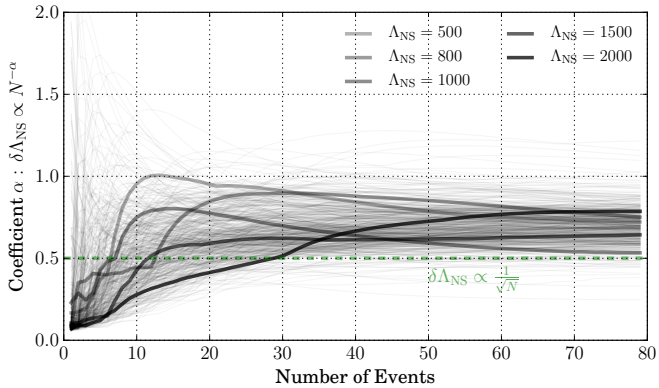


FIG. 11. Assuming a power-law dependence of the measurement error on the number of events:  $\delta\Lambda_{\text{NS}} \propto 1/N^\alpha$ , we show  $\alpha$  in this figure as a function of the number of observed events  $N$ . Shown are five families of 100 population draws each, with each family corresponding to one of  $\Lambda_{\text{NS}} = \{500, 800, 1000, 1500, 2000\}$ . Each grey curve corresponds to one of these  $100 \times 5 = 500$  populations. The thicker curves, one from each family, shows the population we discussed in Fig. 7–8. We find that a power-law is a good approximation for the concerned dependence, and information accumulates *faster* than  $1/\sqrt{N}$ . We estimate  $\alpha \simeq 0.7^{+0.2}_{-0.2}$ .

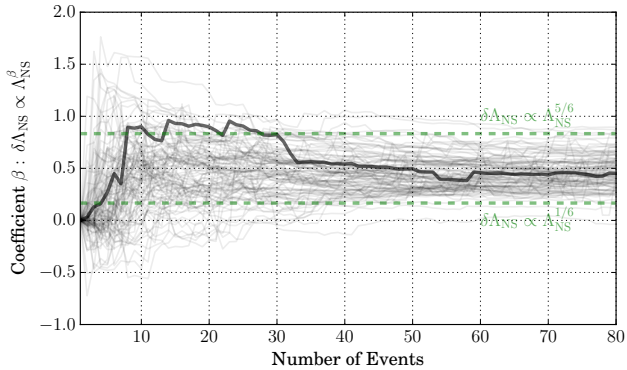


FIG. 12. In this figure, which is similar to Fig. 11, we quantify the dependence of  $\delta\Lambda_{\text{NS}}$  on  $\Lambda_{\text{NS}}$  itself. Of the five families of simulated NSBH populations, we construct 100 independent sets taking one population from each family. With each of these 100 sets, and assuming a power-law dependence:  $\delta\Lambda_{\text{NS}} \propto \Lambda_{\text{NS}}^\beta$ , we estimate  $\beta$  and show it in this figure as a function of the number of observed events  $N$ . We find that  $\beta$  can be estimated to lie within  $[1/6, 5/6]$  with a likely value close to  $1/2$ . Since  $0 < \beta < 1$ , the relative error  $\delta\Lambda_{\text{NS}}/\Lambda_{\text{NS}}$  decreases as the star gets more deformable, while the absolute error  $\delta\Lambda_{\text{NS}}$  increases.

from the least to the most deformable neutron stars. As in the right panel of Fig. 7, the line-circle curves track the median measured  $\Lambda_{\text{NS}}$ , while the filled regions show the associated 90% confidence intervals. From the figure, we observe the following: (i) the shrinkage of confidence interval widths with increasing  $N$  happens in a

similar manner for all populations, (ii) within  $5 – 10$  observations, median measured  $\Lambda_{\text{NS}}$  for all populations lie within  $\pm 10\%$  of the true values, and (iii) it takes approximately 20 events to distinguish definitively (with 90% confidence) between deformable NSs with  $\Lambda_{\text{NS}} = 2000$  and compact NSs with  $\Lambda_{\text{NS}} = 500$ , or equivalently to distinguish between hard, moderate and soft nuclear equations of state. This is comparable to what has been found for monolithic binaries of neutron stars [37–39].

So far we have discussed individual realizations of NSBH populations. The underlying stochasticity of the population generation process makes it difficult to draw generalized inferences (from a single realization) about the measurability of  $\Lambda_{\text{NS}}$ . We mitigate this by drawing multiple realizations of population generation (i.e. multiple identically constructed populations). Fig. 9 shows the first results for multiple populations. Let's focus on the left panel first. We show the median measured value of  $\Lambda_{\text{NS}}$  from 100 independent populations with fixed  $\Lambda_{\text{NS}} = 2000$  as the top set of curves. The one highlighted (in green) curve corresponds to the population discussed above. Similarly, we generate sets of 100 populations with  $\Lambda_{\text{NS}} = 500 – 1500$ , and show the median measured  $\Lambda_{\text{NS}}$  as four distinct groups of curves in Fig. 9 (with the single highlighted curve in each group corresponding to Fig. 7–8). Dash-dotted horizontal lines demarcate  $\pm 50\%$  error intervals around the true  $\Lambda_{\text{NS}}$  values. All of these populations are drawn under paradigm A (i.e. with BH masses allowed to sample the mass-gap that spans  $2 – 5M_\odot$ ). From the figure, we can conclude with a high likelihood that our measured  $\Lambda_{\text{NS}}$  values will be within 10% of the real value in  $15 – 20$  events for less deformable neutron stars with  $\Lambda_{\text{NS}} \leq 1000$ , and in as few as 10 events for more deformable stars with  $\Lambda_{\text{NS}} \geq 1500$ . The right panel of the figure is identical to the left panel, but drawn under population paradigm B (no BHs allowed within the mass-gap). Under this paradigm, we expectedly find that information accumulation is slower. It would take  $20 – 40$  detections with  $\rho \geq 10$  under this paradigm, for our (median) measured  $\Lambda_{\text{NS}}$  to lie within 10% of the true value (fewer for more deformable NSs, as one would expect). This is a promising deduction, as one might expect to see  $\mathcal{O}(10)$  events over a few years' timescale with design aLIGO [55].

Further, we investigate the statistical uncertainties associated with  $\Lambda_{\text{NS}}$  measurements. We use 90% confidence intervals as our measure of the same. The left column of Fig. 10 shows results under paradigm A, where BH mass priors include the mass-gap. In each panel we show the width of the 90% confidence interval measured from  $N$  events (with  $N$  on the  $x$ -axis), normalized by the true value of  $\Lambda_{\text{NS}}$  for the population. In grey are shown results from each of 100 population realizations, with the single population highlighted in color corresponding to the one we focused on in Fig. 7–8. The inset shows the same, except that the ordinate is *not* normalized by the true value of  $\Lambda_{\text{NS}}$ . From top to bottom, the population  $\Lambda_{\text{NS}}$  decreases from  $\Lambda_{\text{NS}} = 2000 \rightarrow 500$ , corresponding to de-

creasingly deformable NSs with softer equations of state. We observe the following: (i) for moderately-hard to hard equations of state with  $\Lambda_{\text{NS}} \geq 1000$ , we can constrain  $\Lambda_{\text{NS}}$  within  $\pm 50\%$  using only 10 – 20 events, and within  $\pm 25\%$  with 25–40 events; (ii) for softer equations of state with  $\Lambda_{\text{NS}} < 1000$ , we will achieve the same accuracy with 20–30 and 50+ events, respectively; and (iii) for the first 5 or so observations, our measurement confidence spans the entire prior allowed range  $\Lambda_{\text{NS}} \in [0, 4000]$ , as shown by the plateauing towards the left edge in each panel’s inset. In the right column, each panel panel is identical to its corresponding left one, with the difference that populations are drawn under paradigm B, which does *not* allow for BH masses to fall within the mass-gap. We find that for NSs with  $\Lambda_{\text{NS}} \leq 1000$ , it would take 25 – 40 events to constrain  $\Lambda_{\text{NS}}$  within  $\pm 50\%$  and 50+ events to constrain it within  $\pm 25\%$ . This is somewhat slower than paradigm A, as is to be expected since here we preclude the lowest mass-ratios, which correspond to signals with largest tidal signatures. For  $\Lambda_{\text{NS}} > 1000$  we find that we can constrain  $\Lambda_{\text{NS}}$  within  $\pm 50\%$  with a similar number of events as for paradigm A, but will need more (30 – 40, as compared to 25 – 40) events to further constrain it to within  $\pm 25\%$  of the true value. These are some of the primary findings of this paper.

Finally, we quantitatively explore the dependence of our statistical uncertainties for  $\Lambda_{\text{NS}}$  on the number of events, as well as on the true NS deformability itself. First, we will focus on the dependence on  $N$ . We assume a power-law dependence of the form  $\delta\Lambda_{\text{NS}} \propto 1/N^\alpha$ . For each of the 100 populations for each of  $\Lambda_{\text{NS}} = 500 – 2000$ , we compute the exponent  $\alpha$  as a function of the number of observed events  $N$ , and show it in Fig. 11. There are  $100 \times 5 = 500$  curves on the figure, with one highlighted for each value of population’s  $\Lambda_{\text{NS}}$ . These highlighted values are only special in the sense that they correspond to populations discussed earlier in this section (c.f. Fig. 7–8). We immediately observe two things, (i) there is a globally similar dependence on  $N$  for all populations, and (ii) information accumulates *faster* than  $1/\sqrt{N}$ . In fact, we find that if  $\delta\Lambda_{\text{NS}} \propto \frac{1}{N^\alpha}$ ,  $\alpha$  lies in the range  $0.7^{+0.2}_{-0.2}$ . Next, we focus on the dependence of  $\delta\Lambda_{\text{NS}}$  on  $\Lambda_{\text{NS}}$  of the population itself. As suggested by Fisher-matrix studies [19], and as for  $N$ , we assume the form  $\delta\Lambda_{\text{NS}} \propto \Lambda_{\text{NS}}^\beta$ . From each set of 100 populations with a given  $\Lambda_{\text{NS}}$  value, we draw one at random, and form a set of 5 similarly drawn populations, one for each of  $\Lambda_{\text{NS}} = \{500, 800, 1000, 1500, 2000\}$ . With each set, we determine  $\beta$  for different number of observed events  $N$ . In all, we make 100 independent 5-population sets and show the value of  $\beta$  measured from each in Fig. 12. We find that the assumed relation  $\delta\Lambda_{\text{NS}} \propto \Lambda_{\text{NS}}^\beta$  gets fairly robust for larger values of  $N$ , with  $\beta$  converging to  $\beta = 0.5^{+0.33}_{-0.33}$ . The fact that  $0 < \beta < 1$  implies that the relative error  $\delta\Lambda_{\text{NS}}/\Lambda_{\text{NS}}$  decreases with increasing  $\Lambda_{\text{NS}}$ , while the absolute error *increases*. From these results, we conclude that the measurement uncertainty for  $\Lambda_{\text{NS}}$

after  $N$  observations is

$$\delta\Lambda_{\text{NS}} \propto \frac{\Lambda_{\text{NS}}^{0.5^{+0.33}_{-0.33}}}{N^{0.7^{+0.2}_{-0.2}}} \quad (11)$$

We also find that while these results are inferred from paradigm A populations, paradigm B gives very similar results.

To summarize, in this section we study the improvement in our measurement of NS deformability parameter  $\Lambda_{\text{NS}}$  with an increasing number of events. We do so by simulating plausible populations of disrupting NSBH binaries (with  $\rho \geq 10$ ). We find that: (i) for more deformable neutron stars (harder equation of states), the median measured value of  $\Lambda_{\text{NS}}$  comes within 10% of the true value with as few as 10 events, while achieving the same accuracy for softer equations of state will take 15 – 20 source detections; (ii) the statistical uncertainty associated with  $\Lambda_{\text{NS}}$  measurement shrinks to within  $\pm 50\%$  with 10 – 20 events, and to within  $\pm 25\%$  with 50+ events, when source  $\Lambda_{\text{NS}} \geq 1000$ ; (iii) for softer equations of state, the same could take 25 – 40 and 50+ events, respectively for the two uncertainty thresholds; and (iv) if BHs really do observe the astrophysical mass-gap, the information accumulation is somewhat slower than if they do not. We conclude that within 20 – 30 observations, aLIGO would begin to place very interesting bounds on the NS deformability, which would allow us to rule out or rank different equations of state for neutron star matter.

## VI. DISCUSSION

The pioneering terrestrial observation of gravitational waves by Advanced LIGO harbinger the dawn of an era of gravitational-wave astronomy where observations, more than theory, would play the driving role. Binaries of compact stellar objects evolve under the radiation reaction force of emitting gravitational waves.

Conventional astronomical methods have, to date, made observations of 2500 NSs with masses between  $1.25 – 2.1M_\odot$  [44, 64–68], although tightly clustered within  $1.35 \pm 0.5M_\odot$  [44]. Observations of over 2500 NSs have shown that the spin of NSs  $|\vec{\chi}_{\text{NS}}|$  have magnitudes that are  $< 1\%$  [45]. On the other hand, indirect observations of stellar-mass BHs place their masses between  $5 – 35M_\odot$ , with their spin angular momenta  $|\vec{\chi}_{\text{BH}}|$  ranging from small to nearly extremal (Kerr) values (see, e.g., Refs. [69–71] for examples of nearly extremal estimates of BH spins, Refs. [72, 73] for recent reviews of astrophysical BH spin measurements, and Figure 5 of Ref. [45] for a comparison of NS and BH spins).

[PK: To be continued after revision of the introduction.]

## ACKNOWLEDGMENTS

Acknowledgments

## REFERENCES

- 
- [1] D. Shoemaker (LIGO Collaboration), “Advanced LIGO anticipated sensitivity curves,” (2010), LIGO Document T0900288-v3.
- [2] B. P. Abbott *et al.* (LIGO Scientific Collaboration, Virgo Collaboration), *Phys. Rev. Lett.* **116**, 061102 (2016), arXiv:1602.03837 [gr-qc].
- [3] J. Abadie, B. P. Abbott, R. Abbott, M. Abernathy, T. Accadia, F. Acernese, C. Adams, R. Adhikari, P. Ajith, B. Allen, and et al. (LIGO Scientific Collaboration, Virgo Collaboration), *Class. Quantum Grav.* **27**, 173001 (2010), arXiv:1003.2480 [astro-ph.HE].
- [4] D. Eichler, M. Livio, T. Piran, and D. N. Schramm, *Nature* **340**, 126 (1989).
- [5] R. Narayan, B. Paczynski, and T. Piran, *Astrophys. J. Lett.* **395**, L83 (1992), astro-ph/9204001.
- [6] R. Mochkovitch, M. Hernanz, J. Isern, and X. Martin, *Nature* **361**, 236 (1993).
- [7] S. D. Barthelmy *et al.*, *Nature* **438**, 994 (2005), arXiv:astro-ph/0511579 [astro-ph].
- [8] D. B. Fox, D. A. Frail, P. A. Price, S. R. Kulkarni, E. Berger, T. Piran, A. M. Soderberg, S. B. Cenko, P. B. Cameron, A. Gal-Yam, M. M. Kasliwal, D.-S. Moon, F. A. Harrison, E. Nakar, B. P. Schmidt, B. Penprase, R. A. Chevalier, P. Kumar, K. Roth, D. Watson, B. L. Lee, S. Shectman, M. M. Phillips, M. Roth, P. J. McCarthy, M. Rauch, L. Cowie, B. A. Peterson, J. Rich, N. Kawai, K. Aoki, G. Kosugi, T. Totani, H.-S. Park, A. MacFadyen, and K. C. Hurley, *Nature* **437**, 845 (2005), astro-ph/0510110.
- [9] N. Gehrels, C. L. Sarazin, P. T. O’Brien, B. Zhang, L. Barbier, S. D. Barthelmy, A. Blustin, D. N. Burrows, J. Cannizzo, J. R. Cummings, M. Goad, S. T. Holland, C. P. Hurkett, J. A. Kennea, A. Levan, C. B. Markwardt, K. O. Mason, P. Meszaros, M. Page, D. M. Palmer, E. Rol, T. Nakamoto, R. Willingale, L. Angelini, A. Beardmore, P. T. Boyd, A. Breeveld, S. Campana, M. M. Chester, G. Chincarini, L. R. Cominsky, G. Cusumano, M. de Pasquale, E. E. Fenimore, P. Giommi, C. Gronwall, D. Grupe, J. E. Hill, D. Hinshaw, J. Hjorth, D. Hullinger, K. C. Hurley, S. Klose, S. Kobayashi, C. Kouveliotou, H. A. Krimm, V. Mangano, F. E. Marshall, K. McGowan, A. Moretti, R. F. Mushotzky, K. Nakazawa, J. P. Norris, J. A. Nousek, J. P. Osborne, K. Page, A. M. Parsons, S. Patel, M. Perri, T. Poole, P. Romano, P. W. A. Roming, S. Rosen, G. Sato, P. Schady, A. P. Smale, J. Sollerman, R. Starling, M. Still, M. Suzuki, G. Tagliaferri, T. Takahashi, M. Tashiro, J. Tueller, A. A. Wells, N. E. White, and R. A. M. J. Wijers, *Nature* **437**, 851 (2005), astro-ph/0505630.
- [10] M. Shibata, M. D. Duez, Y. T. Liu, S. L. Shapiro, and B. C. Stephens, *Phys. Rev. Lett.* **96**, 031102 (2006), arXiv:astro-ph/0511142 [astro-ph].
- [11] V. Paschalidis, M. Ruiz, and S. L. Shapiro, *Astrophys. J.* **806**, L14 (2015), arXiv:1410.7392 [astro-ph.HE].
- [12] N. R. Tanvir, A. J. Levan, A. S. Fruchter, J. Hjorth, R. A. Hounsell, K. Wiersema, and R. L. Tunnicliffe, *Nature* **500**, 547 (2013), arXiv:1306.4971 [astro-ph.HE].
- [13] F. Foucart, E. O’Connor, L. Roberts, M. D. Duez, R. Haas, L. E. Kidder, C. D. Ott, H. P. Pfeiffer, M. A. Scheel, and B. Szilagyi, *Phys. Rev. D* **91**, 124021 (2015), arXiv:1502.04146.
- [14] G. Lovelace, M. D. Duez, F. Foucart, L. E. Kidder, H. P. Pfeiffer, M. A. Scheel, and B. Szilagyi, *Class. Quantum Grav.* **30**, 135004 (2013), arXiv:1302.6297 [gr-qc].
- [15] M. B. Deaton, M. D. Duez, F. Foucart, E. O’Connor, C. D. Ott, L. E. Kidder, C. D. Muhlberger, M. A. Scheel, and B. Szilagyi, *Astrophys. J.* **776**, 47 (2013), arXiv:1304.3384 [astro-ph.HE].
- [16] F. Foucart, *Phys. Rev. D* **86**, 124007 (2012), arXiv:1207.6304 [astro-ph.HE].
- [17] J. Vines, É. É. Flanagan, and T. Hinderer, *Phys. Rev. D* **83**, 084051 (2011), arXiv:1101.1673 [gr-qc].
- [18] K. Kyutoku, M. Shibata, and K. Taniguchi, *Phys. Rev. D* **82**, 044049 (2010), arXiv:1008.1460 [astro-ph.HE].
- [19] B. D. Lackey, K. Kyutoku, M. Shibata, P. R. Brady, and J. L. Friedman, *Phys. Rev. D* **89**, 043009 (2014), arXiv:1303.6298 [gr-qc].
- [20] F. Pannarale, E. Berti, K. Kyutoku, B. D. Lackey, and M. Shibata, (2015), arXiv:1509.06209 [gr-qc].
- [21] F. Foucart, L. Buchman, M. D. Duez, M. Grudich, L. E. Kidder, I. MacDonald, A. Mroue, H. P. Pfeiffer, M. A. Scheel, and B. Szilagyi, *Phys. Rev. D* **88**, 064017 (2013), arXiv:1307.7685 [gr-qc].
- [22] M. Shibata and K. Taniguchi, *Phys. Rev. D* **77**, 084015 (2008), arXiv:0711.1410 [gr-qc].
- [23] V. Ferrari, L. Gualtieri, and F. Pannarale, *Phys. Rev. D* **81**, 064026 (2010), arXiv:0912.3692 [gr-qc].
- [24] K. Kawaguchi, K. Kyutoku, H. Nakano, H. Okawa, M. Shibata, and K. Taniguchi, *Phys. Rev. D* **92**, 024014 (2015), arXiv:1506.05473 [astro-ph.HE].
- [25] W. H. Lee and W. L. Kluzniak, *Astroph. J.* **526**, 178 (1999).
- [26] W. H. Lee and W. L. Kluzniak, *Mon. Not. Roy. Astr. Soc.* **308**, 780 (1999).
- [27] W. H. Lee, *Mon. Not. Roy. Astr. Soc.* **318**, 606 (2000).
- [28] R. Oechslin, H. T. Janka, and A. Marek, *Astron. Astrophys.* **467**, 395 (2007), arXiv:astro-ph/0611047.
- [29] J. S. Read, B. D. Lackey, B. J. Owen, and J. L. Friedman, *Phys. Rev. D* **79**, 124032 (2009), arXiv:0812.2163 [astro-ph].
- [30] C. Markakis, J. S. Read, M. Shibata, K. Uryu, J. D. E. Creighton, and J. L. Friedman, in *On recent developments in theoretical and experimental general relativity, astrophysics and relativistic field theories. Proceedings, 12th Marcel Grossmann Meeting on General Relativity, Paris, France, July 12-18, 2009. Vol. 1-3* (2010) pp. 743-745, arXiv:1008.1822 [gr-qc].
- [31] C. Markakis, J. S. Read, M. Shibata, K. Uryu, J. D. Creighton, *et al.*, *J. Phys. Conf. Ser.* **189**, 012024 (2009), arXiv:1110.3759 [gr-qc].
- [32] N. Stergioulas, A. Bauswein, K. Zagouris, and H.-

- T. Janka, *Mon. Not. Roy. Astr. Soc.* **418**, 427 (2011), arXiv:1105.0368 [gr-qc].
- [33] W. E. East, F. Pretorius, and B. C. Stephens, *Phys. Rev. D* **85**, 124009 (2012), arXiv:1111.3055 [astro-ph.HE].
- [34] B. D. Lackey and L. Wade, *Phys. Rev. D* **91**, 043002 (2015), arXiv:1410.8866 [gr-qc].
- [35] L. Wade, J. D. E. Creighton, E. Ochsner, B. D. Lackey, B. F. Farr, *et al.*, *Phys. Rev. D* **89**, 103012 (2014), arXiv:1402.5156 [gr-qc].
- [36] A. Bauswein, N. Stergioulas, and H.-T. Janka, *Phys. Rev. D* **90**, 023002 (2014), arXiv:1403.5301 [astro-ph.SR].
- [37] W. Del Pozzo, T. G. F. Li, M. Agathos, C. Van Den Broeck, and S. Vitale, *Phys. Rev. Lett.* **111**, 071101 (2013), arXiv:1307.8338 [gr-qc].
- [38] K. Chatzioannou, K. Yagi, A. Klein, N. Cornish, and N. Yunes, *Phys. Rev. D* **92**, 104008 (2015), arXiv:1508.02062 [gr-qc].
- [39] M. Agathos, J. Meidan, W. D. Pozzo, T. G. F. Li, M. Tompitak, J. Veitch, S. Vitale, and C. V. D. Broeck, *prd* **92**, 023012 (2015), arXiv:1503.05405 [gr-qc].
- [40] A. Maselli, L. Gualtieri, and V. Ferrari, *Phys. Rev. D* **88**, 104040 (2013), arXiv:1310.5381 [gr-qc].
- [41] K. Yagi and N. Yunes, *Phys. Rev. D* **89**, 021303 (2014), arXiv:1310.8358 [gr-qc].
- [42] B. D. Lackey, K. Kyutoku, M. Shibata, P. R. Brady, and J. L. Friedman, *Phys. Rev. D* **85**, 044061 (2012), arXiv:1109.3402 [astro-ph.HE].
- [43] M. Vallisneri, *Phys. Rev. D* **77**, 042001 (2008), arXiv:gr-qc/0703086 [GR-QC].
- [44] “stellarcollapse.org – Neutron star mass tables,” <http://www.stellarcollapse.org/nsmasses>.
- [45] M. C. Miller and J. M. Miller, *Phys. Rept.* **548**, 1 (2014), arXiv:1408.4145 [astro-ph.HE].
- [46] C. D. Bailyn, R. K. Jain, P. Coppi, and J. A. Orosz, *Astrophys. J.* **499**, 367 (1998), arXiv:astro-ph/9708032 [astro-ph].
- [47] V. Kalogera and G. Baym, *Astrophys. J.* **470**, L61 (1996), arXiv:astro-ph/9608059 [astro-ph].
- [48] L. Kreidberg, C. D. Bailyn, W. M. Farr, and V. Kalogera, *Astrophys. J.* **757**, 36 (2012), arXiv:1205.1805 [astro-ph.HE].
- [49] T. B. Littenberg, B. Farr, S. Coughlin, V. Kalogera, and D. E. Holz, (2015), arXiv:1503.03179 [astro-ph.HE].
- [50] J. Abadie, B. P. Abbott, R. Abbott, T. D. Abbott, M. Abernathy, T. Accadia, F. Acernese, C. Adams, R. Adhikari, C. Affeldt, and et al., *Astron. Astrophys.* **541**, A155 (2012), arXiv:1112.6005.
- [51] L. P. Singer *et al.*, *Astrophys. J.* **795**, 105 (2014), arXiv:1404.5623 [astro-ph.HE].
- [52] L. P. Singer and L. R. Price, *Phys. Rev. D* **93**, 024013 (2016), arXiv:1508.03634 [gr-qc].
- [53] C. Pankow, P. Brady, E. Ochsner, and R. O’Shaughnessy, *Phys. Rev. D* **92**, 023002 (2015), arXiv:1502.04370 [gr-qc].
- [54] F. Foucart, M. B. Deaton, M. D. Duez, L. E. Kidder, I. MacDonald, C. D. Ott, H. P. Pfeiffer, M. A. Scheel, B. Szilagyi, and S. A. Teukolsky, *Phys. Rev. D* **87**, 084006 (2013), arXiv:1212.4810 [gr-qc].
- [55] J. Abadie *et al.* (LIGO Scientific Collaboration), *Class. Quantum Grav.* **27**, 173001 (2010), arXiv:1003.2480 [gr-qc].
- [56] F. Pannarale, E. Berti, K. Kyutoku, B. D. Lackey, and M. Shibata, *Phys. Rev. D* **92**, 084050 (2015), arXiv:1509.00512 [gr-qc].
- [57] A. Taracchini, Y. Pan, A. Buonanno, E. Barausse, M. Boyle, T. Chu, G. Lovelace, H. P. Pfeiffer, and M. A. Scheel, *Phys. Rev. D* **86**, 024011 (2012), arXiv:1202.0790 [gr-qc].
- [58] A. Buonanno and T. Damour, *Phys. Rev. D* **59**, 084006 (1999), arXiv:gr-qc/9811091 [gr-qc].
- [59] A. Taracchini, A. Buonanno, Y. Pan, T. Hinderer, M. Boyle, D. A. Hemberger, L. E. Kidder, G. Lovelace, A. H. Mroue, H. P. Pfeiffer, M. A. Scheel, B. Szilagyi, N. W. Taylor, and A. Zenginoglu, *Phys. Rev. D* **89** (R), 061502 (2014), arXiv:1311.2544 [gr-qc].
- [60] M. Prrer, (2015), arXiv:1512.02248 [gr-qc].
- [61] P. Kumar, K. Barkett, S. Bhagwat, N. Afshari, D. A. Brown, G. Lovelace, M. A. Scheel, and B. Szilgyi, *Phys. Rev. D* **92**, 102001 (2015), arXiv:1507.00103 [gr-qc].
- [62] P. Kumar, T. Chu, H. Fong, H. P. Pfeiffer, M. Boyle, D. A. Hemberger, L. E. Kidder, M. A. Scheel, and B. Szilagyi, (2016), arXiv:1601.05396 [gr-qc].
- [63] M. Prrer, M. Hannam, and F. Ohme, (2015), arXiv:1512.04955 [gr-qc].
- [64] A. Lyne, M. Burgay, M. Kramer, A. Possenti, R. Manchester, *et al.*, *Science* **303**, 1153 (2004), arXiv:astro-ph/0401086 [astro-ph].
- [65] P. Demorest, T. Pennucci, S. Ransom, M. Roberts, and J. Hessels, *Nature* **467**, 1081 (2010), arXiv:1010.5788 [astro-ph.HE].
- [66] J. Antoniadis, P. C. C. Freire, N. Wex, T. M. Tauris, R. S. Lynch, M. H. van Kerkwijk, M. Kramer, C. Bassa, V. S. Dhillon, T. Driebe, J. W. T. Hessels, V. M. Kaspi, V. I. Kondratiev, N. Langer, T. R. Marsh, M. A. McLaughlin, T. T. Pennucci, S. M. Ransom, I. H. Stairs, J. van Leeuwen, J. P. W. Verbiest, and D. G. Whelan, *Science* **340**, 448 (2013), arXiv:1304.6875 [astro-ph.HE].
- [67] “Australia Telescope National Facility – catalog,” <http://www.atnf.csiro.au/research/pulsar/psrcat/>.
- [68] “McGill Online Magnetar Catalog,” <http://www.physics.mcgill.ca/~pulsar/magnetar/main.html>.
- [69] J. E. McClintock, R. Shafee, R. Narayan, R. A. Remillard, S. W. Davis, and L.-X. Li, *Astrophys. J.* **652**, 518 (2006).
- [70] J. Miller, C. Reynolds, A. Fabian, G. Miniutti, and L. Gallo, *Astrophys. J.* **697**, 900 (2009), arXiv:0902.2840 [astro-ph.HE].
- [71] L. Gou, J. E. McClintock, R. A. Remillard, J. F. Steiner, M. J. Reid, *et al.*, *Astrophys. J.* **790**, 29 (2014).
- [72] J. E. McClintock, R. Narayan, and J. F. Steiner, *Space Sci. Rev.* **183**, 295 (2014), arXiv:1303.1583 [astro-ph.HE].
- [73] C. S. Reynolds, *Space Science Reviews* **183**, 277 (2014), arXiv:1302.3260 [astro-ph.HE].